NOTE TO USERS

Adaptive Control for Frictional and Impact Chatter in Metal Cutting via Piezoelectric Actuator

Yang Wang

A Thesis

in

The Department

of

Mechanical and Industrial Engineering

Presented in Partial Fulfilment of the Requirements
for the Degree of Master of Science at
Concordia University
Montreal, Quebec, Canada

June 2003

Your file Votre référence
ISBN: 0-612-91135-7
Our file Notre référence
ISBN: 0-612-91135-7

Abstract

Adaptive Control for Frictional and Impact Chatter in Metal Cutting via Piezoelectric Actuator

Yang Wang

From the very beginning, metal cutting has had one troublesome obstacle in increasing productivity and accuracy, namely chatter. In machining, chatter is perceived as unwanted excessive vibration between the tool and workpiece, resulting in a poor surface finish and accelerated tool wear. It also has a deteriorating effect on the machine tool life, and the reliability and safety of the machining operation. The frictional and impact chatter are mainly due to the nonlinearity of the dry friction and the intermittent contact between the cutting tool and the workpiece. This thesis addresses the controller design for suppressing frictional and impact chatter in metal cutting systems.

Piezoelectric actuators have become a standard option in positioning applications where the displacements must be small and highly accurate. In particular, ultra-precision manufacturing requires exceptionally fine and repeatable motions, making piezoelectric actuators a common choice. In this thesis, with the application of piezoelectric actuators in two directions x and y, an adaptive controller is developed to deal

with unknown hysteresis combined with time delay. And an approach for adaptive control of frictional and impact chatter for metal cutting by piezoelectric actuator is presented. The developed control approach is based on an accepted model of the metal cutting process dynamics in the context of an approximate analysis of the resulting non-linear differential equations of motion. The stability analysis of the system is also given. The results of the numerical study of the adaptive control system shows the effectiveness of control of frictional and impact chatter with piezoelectric actuators.

Dedication

This thesis is dedicated to my beloved parents Fa Ji Wang, Yin Yu Jiao and my sister Jun Wang. Without their permanent love, support and believing in me this work would have not been possible.

Acknowledgement

I would like to express my sincere appreciation and gratitude to my advisors Dr. Chun-Yi Su and Dr. Henry Hong. It was only under their constant patient guidance and support that I could successfully overcome many difficulties. Moreover, their characters of hardworking people with a precise attitude of work, optimism, sense of humor and their readiness to help other people had a great influence on me and will be my constant inspiration in future endeavors.

I would also like to thank my friends in Montreal, in particular my roommates Chaohui Sun and Yu Gu, Zhu Jun, Chao Chen, Tao Zhou, Feng Hu, Xiaoniu Dai and Yi Zhao. Being with them makes my life in Montreal for the past two years full of fun.

Contents

List of Figures

Nomerclature

c_{1-4} = cutting process constants

c_x, c_y = stiffness in x and y direction

C_1 = Ritz constant

$f()$ = vector of force

$f_{i,cut}$ = ith component of the cutting force

f_0- vector of other forces acting on the machine tool structure

f_x, f_y = cutting force in x and y direction resppectively

h = depth of cut

h_0 = initial depth of cut

$H()$ = Heaviside function

k_x, k_y = viscous damping in x and y direction

m = mass of the vibrating system

q_0 = modulus of the cutting force

R = variable shear plastic deformation coefficient

R_0 = shear plastic deformation constant

t = time

v_f = relative velocity between the tool and the workpiece in y direction

v_0 = velocity of the workpiece

v_r = relative velocity between the tool and the workpiece in x direction

x, y = model's coordinates

α = stiffness ratio

α_j = jth cutting parameter

ϕ = shear angle

$\chi()$ = friction coefficient of a chip on the ranke surface

ξ = coefficient of viscous damping

ξ_x, ξ_y = coefficient of viscous damping in x and y direction respectively

ω_{0x}, ω_{0y} = natural frequency in x and y direction respectively

μ_0 = static friction coefficient

Δt = time step

Chapter 1

INTRODUCTION

1.1 General

Machining (turning, milling, drilling) is the most widespread metal process in the mechanical manufacturing industry. Worldwide investment in metal-machining machine tools holds steady or continues to increase year by year. Machining is still the fundamental manufacturing technique and it is expected to remain so for the next few decades. Moreover, it is predicted that ultra-precision machining will take an even more significant role among other manufacturing techniques. [47]

In the search for a significant improvement in accuracy and productivity of machin-

ing processes, the mechanics of chip formation has been revisited in order to understand functional relationships between the process and the technological parameters. This has led to the necessity of considering the chip-formation process to be highly nonlinear with complex interrelations between its dynamics and thermodynamics. However, the major requirement is to perform the technological operation under chatter-free conditions. In machining, chatter is perceived as unwanted excessive vibration between the tool and the workpiece. Piezoelectric actuators have become a standard option in positioning applications where the displacements must be small and highly accurate. In particular, ultra-precision manufacturing requires exceptionally fine and repeatable motions, making piezoelectric actuators an appropriate and common choice.

1.2 Problem Statement

Large relative vibrations between the tool and the workpiece in metal cutting processes can compromise the productivity and accuracy of this manufacturing technique. This is particulary dangerous when a sudden and uncontrolled rise of vibration amplitude occurs. An example of such behavior is self-excited oscillations so-called chatter.

In machining, chatter is perceived as unwanted excessive vibration between the tool and the workpiece resulting in a poor surface finish and accelerates tool wear. It also has a deteriorating effect on the machine tool life and the reliability and safety of the machining operation. The frictional and impact chatter is primary chatter and is mainly due to the nonlinearity of the dry friction and the intermittent contact between the cutting tool and the workpiece.

1.3 Thesis Outline

The main objective of this thesis is to design an adaptive control system to overcome the frictional and impact chatter via piezoelectric actuator. Respecting to the dynamics of the metal cutting system, two mathematic models, namely Deterministic and Stochastic model, are used in this thesis to describe the dynamics of orthogonal cutting in the lathe operation. And the method of Adaptive Control of a Class of Nonlinear Systems with Unknown Backlash-Like Hysteresis is used to develop corresponding control laws to overcome the frictional and impact chatter during the orthogonal cutting process.

The work carried out and the results obtained are organized in this thesis as follows:

Chapter 2 gives the literature review that consists of four parts: 1) Chatter Mechanisms, 2) Metal Cutting Mechanics, 3) Chatter Suppression in Turning 4) Contributions of the Thesis. The first part gives a brief review of chatter mechanisms. Because the chatter mechanism should take into account kinematics, dynamics and geometry of the chip formation, in part 2 the metal cutting mechanics are reviewed. In part 3, preview works of chatter suppression is shown. And in part 4, the comparison of models and control systems for chatter are discussed. The advantages of the model for frictional and impact chatter, piezoelectric actuator and adaptive control of nonlinear system with unknown hysteresis are also discussed.

In Chapter 3 the piezoelectric actuator is introduced. As some advantages of a piezoelectric actuator, such as lager force generation, sub-millisecond response, fast expansion, sub-nanometer resolution and so on, are shown to be suitable in controlling chatter in metal cutting. Finally a continuous-time dynamic model is used to describe the dynamics of piezoelectric actuator.

Chapter 4 fully analyzes the frictional and impact chatter in the two-degree-of-freedom deterministic model. The deterministic model describes dynamic interactions

in the uncoupled MT(Machine Tool)-CP(Cutting process) system in a comprehensive manner.

In Chapter 5 an adaptive control method is developed for the deterministic model. The adaptive control law for nonlinear systems with hysteresis is used in the suppression of chatter because of the inherent hysteresis in piezoelectric actuators. The simulation results of the control system are discussed in this chapter.

Chapter 6 fully analyzes the frictional and impact chatter in the two-degree-of-freedom stochastic model. This chapter demonstrates the necessity of modelling the stochasticity of the cutting process. In particular, the randomness of the specific cutting resistance is examined. The simulation shows the effect of random material property on the vibration of machine tools in the metal cutting process.

In Chapter 7 the adaptive control method for the stochastic model is developed. And the results of simulation of the control system are discussed in this chapter.

Finally, Chapter 8 consists of two parts; 1)Conclusion. This part presents highlight of the present investigation and important conclusions of this studies. 2)Future Works.

This part gives a list of recommendation for further work in this area.

Chapter 2

LITERATURE VIEW

2.1 Chatter Mechanisms

It is possible for periodic force variations in the cutting process to interact with the dynamic stiffness characteristics of the machine tool including the tool holder and workpiece to create vibrations during processing that are known as chatter. This is particularly dangerous when sudden and uncontrolled rise of vibration amplitude occurs. Chatter leads to poor surface finish, dimensional errors in the machined part and also accelerates tool failure. Although chatter can occur in all machining processes (because no machine tool is infinitely stiff), it is a particular problem in operations requiring large length-to-diameter ratio tool holders (for example in bor-

ing deep holes or end milling deep slots and small radius corners in deep pocket) or when machining thin-walled components. It can then be hard to continue the operation because of chatter vibration. The purpose of chatter vibration modelling is to support chatter avoidance strategies. Although the conditions in which such an instability appears can be explained by linear dynamics in many practical situations, more comprehensive insight can be gained only if the dynamic interactions between the machine tool (MT) and the cutting process (CP) are treated as nonlinear.

Despite the continuing effort in the field and generation of new theories [1], [4], [7], [10],[11], [12],[16],[17], [18],[24],[26],[41], there is no consistent explanation for the existence of chatter. The reason behind it is the complexity of the chip-formation process, where the following strongly nonlinear phenomena are interrelated and dependent: temperature-dependent plasticity; temperature and velocity-dependent friction; nonlinear stiffness of machine tools; regenerative effects; and intermittency of the cutting process.

The first attempts to describe chatter were made by Arnold [1], Hahn [11] and Doi & Kato [7]. There have been several theories put forward to explain them, however, a sufficient agreement between different investigators has not been reached yet

(Jemielniak [16]). One reason for these divergences is because of the approach, which treats the dynamics and cutting process separately. Tobias [41], Opitz and Bernardi [29], and Tlusty [40] have abolished the validity of this assumption by observing the intermittent cutting process, and Grabec [10] did the first numerical investigation. Another common example is the existence of the stick-slip phenomena in the machine tool slide ways, which has a great influence on the cutting process itself (Wiercigroch [46]).

The metal cutting process involves a number of strongly nonlinear phenomena, which can be classified into two distinct dynamical systems, namely mechanics and thermodynamics of chip formation. In figure 2.1 the functional interrelationships between these two systems are shown in a form of a close-loop model. The mechanical part is comprised of two major blocks: the cutting and thrust force generation mechanism (CTFGM) and the machine-tool (MTS).The thermodynamical part consists of two blocks: the heat-generation mechanism (HGM) and thermodynamically equivalent chip volume (TECV). The HGM is fed with the initial values of shear flow stress σ_0, friction angle τ_0 and shear angle ϕ_0, and a feedback path of current temperature of the chip, $\theta(t)$. TECV system shows that the equivalent changes of the chip volume due to temperature variations. The input $Q_g(t)$ is the quantity of heat from HGM.

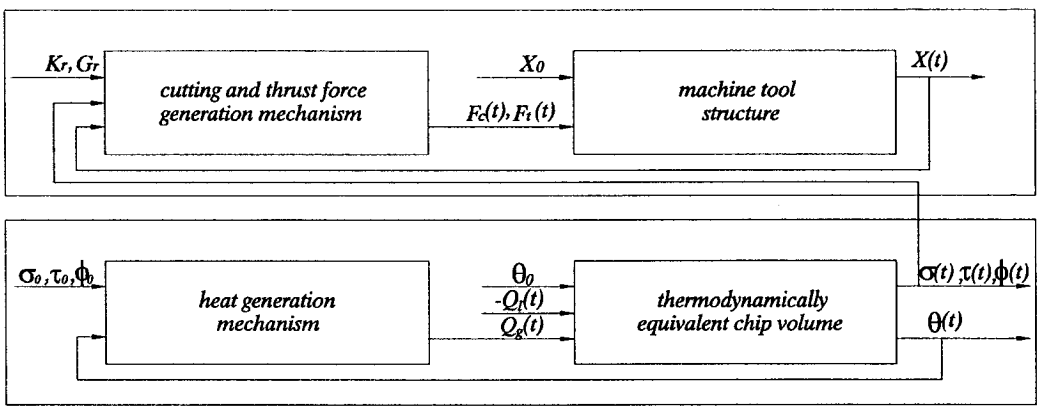

Figure 2.1: Closed-loop model of dynamic and thermodynamic interaction [47]

The input $Q_l(t)$ is the quantity from outside and the cooling system, so it is minus.

The inputs to the CTFGM are the required geometry of the cutting system, G_r, and kinematics of the cutting system, K_r, a feedback from the MTS in a form of the dynamical vector $X(t)$, and a feedback from the thermodynamically equivalent chip volume (TECV) in the form of the shear flow stress, $\sigma(t)$, and the friction and shear angles, $\tau(t)$ and $\phi(t)$. The outputs from CTFGM are the cutting and thrust forces, $F_c(t)$ and $F_t(t)$, which, together with the vector of initial conditions, X_0, act on the MTS, producing the dynamic vector of displacement and velocities, $X(t)$.

From the work of Merritt [26], Kegg [18] and Kudinov [19] the idea of portraying the

dynamic interactions in the metal cutting as a system of automatic control originated. But, all three have only looked at the mechanical part of the problem, and assumed a linear system.

Grabec [10], and Lin & Weng [23] considered mechanical models with nonlinear cutting forces. Recent investigations into nonlinear dynamics show the existence and the importance of chaotic motion (The motion is chaotic, not following any discernable regular pattern but varying in an unpredictable way.), which occurs in many applications. However they are mostly dedicated to the continuous problems. Although some discontinuous systems have been analyzed, e.g., a piecewise oscillator by Shaw and Holmes [35], impact system by Nordmark [28], rotor systems with clearances by Neilson and Gonsalvez [27], only a very few works have been addressed to the dynamics of the cutting process. Preliminary theoretical works carried out by Grabec [10] and Wiercigroch [46] have shown some evidence of chaotic vibrations, which are mainly due to the nonlinearity of the cutting tool and workpiece.

In general, chatter can be classified as primary and secondary. Another classification distinguishes frictional, regenerative, mode-coupling and thermo-mechanical chatter. The following section explains these classifications of chatter.

2.1.1 Frictional Chatter

The distinction between primary (frictional) and secondary (regenerative) chatter can be made easily. Marui et al.[24] compared the size and orientation of the vibratory locus (trajectory of the cutting edge) for the frictional and regenerative chatter. The regenerative locus is almost ten times bigger than the frictional locus and also as their spatial orientations are different [24].

The analytical and experiment studies on the primary chatter reveal that the excitation energy is generated from the friction force both between the workpiece and tool flank and between the chip and the rake surface (Hamdan & Bayoumi [12]). The friction force on the tool face is generally considered to be the force required to shear the welds formed between the sliding surfaces. Because the shear stress varies with the temperature and the shear rate, the friction force can be estimated depending on the cutting velocity. By analyzing the results presented by Cook [26], it is shown that the shear flow stress and the friction force decrease with an increase of chip velocity. Therefore, if there are relative oscillations between the cutting tool and the chip, there will be a net energy input to the system, which can sustain the vibration.

2.1.2 Regenerative Chatter

The most commonly studied form of chatter is known as regenerative chatter. It can occur when compliance of the machine tool structure allows cutting force to displace the cutting edge normal to the cut surface and when, as is common, the path of a cutting edge over a workpiece overlaps a previous path.

Regenerative chatter is the most common form of self-induced vibration. Boothroya [2] had found that the regenerative chatter occurs so often because the majority of cutting involve overlapping cuts and the amplitude of the forced vibrations resulting from shaving a wavy surface from the pervious cut can be significantly amplified although the machine tool system is stable itself. Marui et al. [24] and Kaneko [17] had provided clear evidence of how dominating the regenerative effect can be when compared with other types of chatter by experiments. The cutting force could be a function of the depth of cut,h, the rake angle, α, and clearance angle, β,(Kudinov [19]) which can be written as

$$F_c = F_c(h, \alpha, \beta) \tag{2.1}$$

Assuming that this function has a total differential, Kudinov [19] proposed a formula

for the dynamic variation of the cutting force in the following form:

$$dF_c = \frac{\partial F_c}{\partial h}dh + \frac{\partial F_c}{\partial \alpha}d\alpha + \frac{\partial F_c}{\partial \beta}d\beta \tag{2.2}$$

Tobias & Fishwick [41] adopted a similar approach of modelling the dynamic variation of the cutting force, where the cutting force in turning was assumed to be a function of the depth of cut, h, the feed rate, r, and the rotational speed, Ω, representing the cutting speed, v_c. The formula can be written as

$$dF_c = \frac{\partial F_c}{\partial h}dh + \frac{\partial F_c}{\partial r}dr + \frac{\partial F_c}{\partial \Omega}d\Omega \tag{2.3}$$

where

$$dh = x(t) - \mu x(t - T) \tag{2.4}$$

μ is the factor of overlapping between the previous and present cuts, and T is a period of one revolution.

2.1.3 Mode Coupling

The mode-coupling chatter exists if the vibration in the thrust force direction generates vibration in the cutting force direction and vice versa. This results in simultaneous vibration in the cutting and thrust force direction. Physically, many sources can cause mode-coupling chatter. The sources includes chip thickness variation (Tlusty & Ismail [40]), shear angle oscillations (Wu [43]), regeneration effect (Jemielniak &

Widota [16]), and friction on the rake and clearance surface (Cook [4] and Wiercigroch [46]). The necessary condition is that the cutting and thrust forces have components (feedback) of other direction (Wu & Liu [44]). This has been elegantly captured for a two-degree-of-freedom model by Wu & Liu [44] shown in figure 2.2. The cutting and thrust forces are given by two formulaes, respectively as:

$$m\ddot{x}+c_x\dot{x}+k_xx = 2\omega\sigma_s(x_0-x)[(A_x-C_xv_0)+\frac{1}{2}B_x(\dot{x}-\dot{x}_0)-\frac{1}{2}C_x(\dot{y}-\dot{y}_0)]-\frac{K\omega}{v_c}\dot{x} \quad (2.5)$$

$$m\ddot{y}+c_y\dot{y}+k_yy = 2\omega\sigma_s(x_0-x)[(A_y-C_yv_c)+\frac{1}{2}B_y(\dot{x}-\dot{x}_0)-\frac{1}{2}C_y(\dot{y}-\dot{y}_0)] \quad (2.6)$$

where m is the equivalent vibrating mass, c_x and $c_y$the viscous damping coefficients, k_x and k_y the machine structure stiffness constants, v_c the cutting speed, and K is the damping coefficient evaluated from the ploughing force acting on the tool nose, ω is the frequency, σ_s is shear stress. x_0 and y_0 are the starting position of chip on the surface of workpiece. x and y are the position of tool. F_l and F_c are the cutting forces in x and y directions. The remaining constants in (2.5) and (2.6) (A_x, A_y, B_x, B_y, C_x and C_y) are called the dynamic force coefficients and are fully described in Wu & Liu [43].

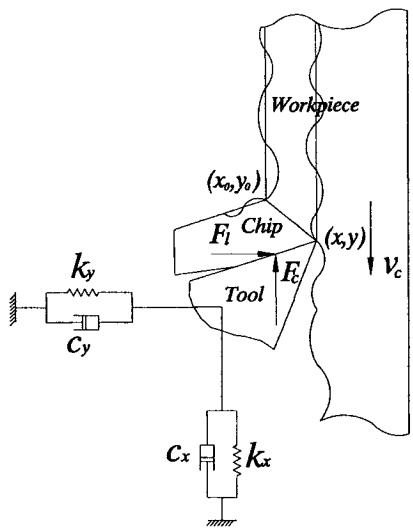

Figure 2.2: Two-degree-of-freedom model of the metal-cutting system

2.1.4 Thermomechanical Chatter

Thermomechanical chatter is due to temperature variations and the temperature distortion of the chip. The first approach to comprehensively describe the thermomechanics was made by Hastings et al. [13]. Shown in the Figure 2.3, the thermodynamical part consists of two blocks: the heat-generation mechanism (HGM) and thermodynamically equivalent chip volume (TECV). The HGM is fed with the initial values of σ_0, τ_0 and ϕ_0, and a feedback path of current temperature of the chip, $\theta(t)$. TECV system shows that the equivalent changes of the chip volume due to temperature variations. The input $Q_g(t)$ is the quantity of heat from HGM. The input $Q_l(t)$

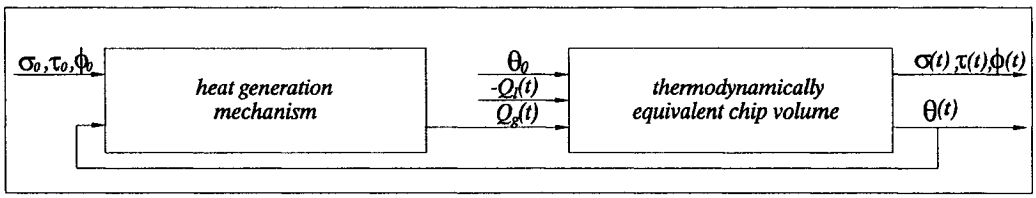

Figure 2.3: Resource of thermomechanical chatter

is the quantity from outside and the cooling system, so it is minus. The output of the HGM are the shear flow stress, $\sigma(t)$, and the friction and shear angles, $\tau(t)$ and $\phi(t)$

They formulated an approximate theory which was applied to two plain carbon steels by using the flow stress data obtained from high-speed cutting and a good agreement between theory and experiment has been shown for predicting the cutting and thrust forces, to account for the effects of temperature and strain-rate in the plastic deformation zone on the mechanics of chip formation.

In the paper by Hastings et al.[13] an approach explaining the influence of the temperature and the strain rate dependent properties of the workpiece has been given. Applying the appropriate stress equilibrium equation along the shear plane, it can be shown that for $0 < \phi \leq \pi/4$, the auxiliary angle, κ, which is the angle between the

shear force F_s and the resultant force R, is given by

$$tan(\kappa) = 1 + 2(\pi/4 - \beta) - Cn \tag{2.7}$$

There are two constants in this equation, in which C is an empirical constant and n is the strain-harding index.

C came from detailed studies of deformed grids in experimental work and calculations of the primary shear strain rate:

$$\dot{\gamma}_s = \frac{Cv_s}{h_0 sin\phi} \tag{2.8}$$

in which $\dot{\gamma}_s$ is the maximum shear strain-rate at the shear plane, v_s is the shear velocity, h_0 is the initial depth of cut.

Strain-hardening index n can be calculated from the empirical strain-stress relation

$$\sigma_s = \sigma_1(\theta_{int}, \dot{\gamma}_{int}), \epsilon^n, \tag{2.9}$$

where σ_s and ϵ are the uniaxial flow stress and strain and σ_1 is a constant defining the stress-strain curve for given values of strain rate, $\dot{\gamma}$, and temperature, θ. The temperature on the shear plane can be calculated by knowing the initial temperature of the workpiece, θ_w, from the following equation,

$$\theta_s = \theta_w + \eta \frac{1 - \psi(v_c)}{\rho S h_0 \omega} \frac{F_s cos\alpha}{cos(\phi - \alpha)} \tag{2.10}$$

in which $\eta \in (0,1)$ is a coefficient accounting for how much of the plastic deformation has occurred on the shear plane, ρ and S are the density and specific capacity of the workpiece, respectively, and $\psi(v_c)$ is the empirical non-dimensional function used to determine a portion of the heat conducted into the workpiece from the shear zone. In a similar manner, the average temperature at the cutting-tool-chip interface, θ_{int}, is calculated

$$\theta_{int} = \theta_w + \frac{1-\psi(v_c)}{\rho S h_0 \omega} \frac{F_s cos\alpha}{cos(\phi-\alpha)} + \xi\theta_m \tag{2.11}$$

where θ_m is the maximum temperature rise in the chip and $\xi \in (0,1)$ is a constant allowing θ_{int} to have an average value. The average temperature rise in the chip, θ_c, and the thickness of the plastic zone, δ, can be calculated from a combination of numerical and empirical formulae,

$$\theta_c = \frac{F sin\phi}{\rho S h \omega cos(\phi-\alpha)} \tag{2.12}$$

$$lg\left(\frac{\theta_m}{\theta_c}\right) = 0.06 - 0.196\delta\left(\frac{R_\theta h}{l}\right)^{0.5} + 0.5lg\left(\frac{R_\theta h}{l}\right) \tag{2.13}$$

where δ is the ratio between the thickness of the plastic zone in the chip and the chip thickness, R_θ is a non-dimensional thermal coefficient and l is the cutting-tool-chip contact length, which can be calculated from the moment equilibrium on the shear plane,

$$l = \frac{h_0 sin\kappa}{cos\lambda sin\phi}\left(1 + \frac{Cn}{3(1+0.5\pi-2\phi-Cn)}\right) \tag{2.14}$$

A relation for the maximum shear strain rate at the cutting-tool-chip interface is given

$$\dot{\gamma}_{int} = \frac{v_c}{\delta h} \frac{sin\phi}{cos(\phi - \alpha)} \tag{2.15}$$

It is the first time that the Hastings' models allows calculation of the temperature and the strain rate at the cutting-tool-chip interface and the corresponding shear flow stress and describe the thermomechanical chatter.

2.2 Metal Cutting Mechanics

In 1800s studies on metal cutting had been carried out. A lot of works have been done in this area[2], [6], [13], [23], [25], [32], [43], [44]. In general, the cutting process is a result of the dynamic interaction between the machine tool, the cutting tool and the workpiece. Therefore, its mathematical description should take into account its kinematics, dynamics, geometry of the chip formation and workpiece, mechanical and thermodynamical properties. A simplified schematic locating all important phenomena in the cutting zone is shown in Figure 2.3 [47]. Here most of the phenomena listed are strongly nonlinear and interdependent. Then the Merchant's model and Hasting's model will be introduced.

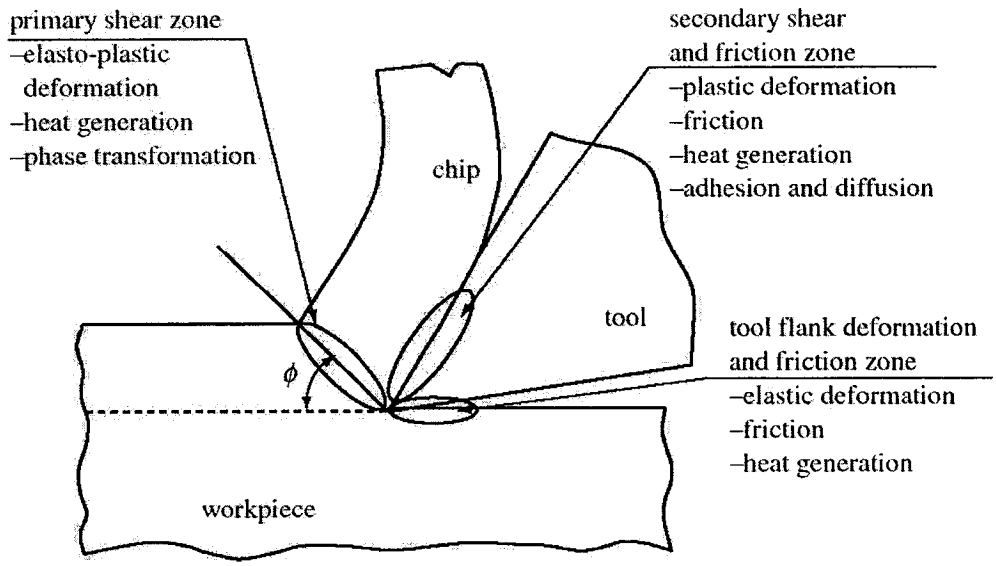

Figure 2.4: Physical phenomena in the cutting zone [47]

2.2.1 Merchant's Model

In the pioneering work of Merchant [25], a model of the cutting process was used in which the shear in chip formation was confined to the shear plane, and movement of the chip over the tool occurred by classic sliding friction, defined by an average friction angle β. Here the uncut layer (initial depth of cut), h_0, of the workpiece in the form of a continuous chip without a built-up edge is seen to be removed along the shear plane. Merchant's force circle were restricted to a model of orthogonal or two-dimensional metal cutting shown in Figure 2.5 [25].

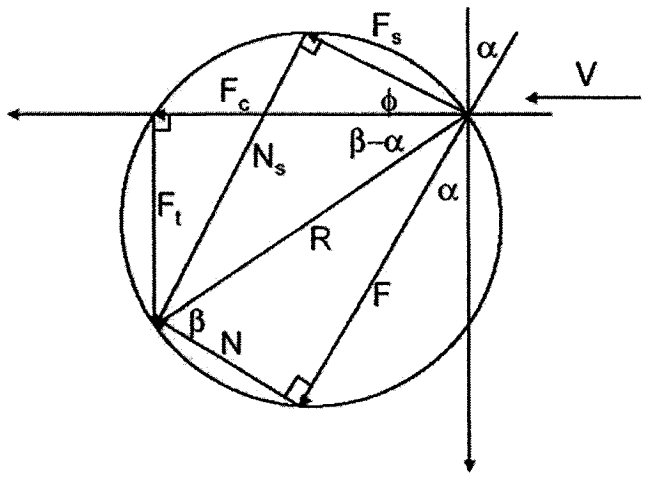

Figure 2.5: Merchant's force diagram [25]

The cutting and feed forces can be found from figure 2.5 as the two equations below:

$$F_c = \frac{h_0\, w\, k\, cos(\beta - \alpha)}{sin\phi\, cos(\phi + \beta - \alpha)} \tag{2.16}$$

$$F_t = \frac{h_0\, w\, k\, sin(\beta - \alpha)}{sin\phi\, cos(\phi + \beta - \alpha)} \tag{2.17}$$

where β is an average friction angle. Appendix A describes Mechant's work in more detail.

2.2.2 Hasting's and Oxley's Models

The main deficiency of the models by Merchant was a difficulty to verify the theoretical predictions with experiments. In the paper by Recht [32] a brief description of the

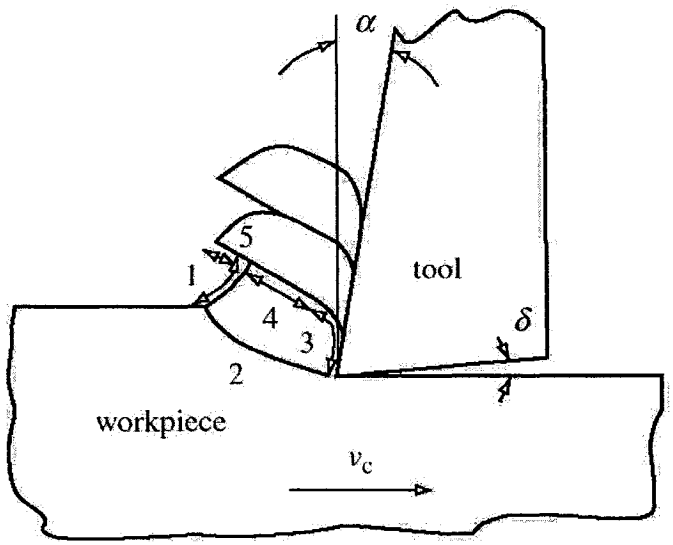

Figure 2.6: Schematic of the segmented chip formation [47]

chip-fragmentation hypothesis is given to illustrate the complexity of this problem.

For certain temperatures and workpiece materials, mechanical properties are not capable of sustaining a steady-stress field and chip segmentation, and the resulting fluctuating stress and temperature fields occur. Referring to Figure 2.6, as the workpiece is approached by the tool, it experiences a stress field, which changes with time. The chip segment enclosed within lines 1, 3, 4 and 5 is being plastically deformed by the tool, and stress, strain and temperature fields are building up in the workpiece. As the material begins to shear along line 5, these fields develop conditions leading to thermoplastic instability, and a very thin shear-localized band absorbs the bulk of

further strain. Then the chip segment moves up the ramp formed by the workpiece material on the workpiece side of line 5. As the tool moves into the ramp, a new segment begins to form. Its upper surface, represented by line 5, becomes the surface through which the tool upsets the material. As upsetting progresses, this surface becomes that identified by line 3 and 4, the latter of which is being pressed against the tool face. Until a new localized shear zone forms due to thermostatic instability, the increasing portion of line 4 (a hot sheared surface) that lies on the rake face remains at rest. Shearing between segments along line 3 ceases when the next localized shear zone forms along line 5, due to the build-up of the stress, strain and temperature fields. Once deformation and shearing have ceased, the chip segments pass up the rake face. Chip-sliding behavior on the rake face is therefore characterized by a start-stop motion. Considering the pressures, temperatures and heat transfer conditions at the cutting-tool-chip interface, sliding resistance would be expected to be much greater for the segmented chips than for continuous chips. When frictional forces and speed are sufficient to produce localized melting temperatures at asperities within the cutting-tool-chip interface, segmented chips produce much higher friction coefficients, interface temperature and tool wear rates than the continuous chips do. As described above, segmented chips experience stick-slip motion. Under very high compression, molten regions in the interface may quench and freeze. Weld bonds in the interface

must be sheared, producing high friction forces.

Unlike most of the classic models of chip formation, such as Merchant's model, Oxley [30] has confirmed that a shear-zone model is much closer to practical machining situation than a shear-plane model. Rather than on a single plane in Oxley's model chip formation is considered to take place in a fan-shaped zone at low speed, and a parallel-sided zone at high speeds. The frictional conditions are described as shear within a layer of the chip adjacent to the rake face of the tool.

2.3 Chatter Suppression in Turning

In order to suppress the chatter in turning, a lot of researches have been done [3], [5], [8], [9], [15], [21], [31], [37], [39]. Rasmussen *et. al.* [31] improved the workpiece surface by employing a digital repetitive servo control with the design of piezoelectric actuated cutting tool. Tarng and Wang [39] developed an adaptive fuzzy control system for the turning processes with highly nonlinear and time-varying cutting characteristic. Shiraishi *et. al.* [37] obtained satisfactory chatter vibration control by implemented optimal control of chatter. Hwang *et. al* [14] implemented a fixed

gain PI control and an adaptive pole assignment control technique with the feed force feedback. Chen and Chang [3] considered the system to be linear with nonlinear time-varying perturbation and employed PI controller to treat this stabilization problem. Recently, with the advantages of piezoelectric actuator, more and more researchers pay attention to the application of piezoelectric actuator for metal cutting systems [5], [8], [9], [15], [21].

2.4 Contributions of the Thesis

2.4.1 Dynamic Model

Early work done by Merchant [25]and his followers examined the relationship between the forces and the chip, and linearity of the machine tool. Recent research conducted by Hastings et al. [13] still followed this line, although theoretically these studies were better founded. According to my knowledge, the problem of relative vibration between the workpiece and the tool in these researches [2], [6], [13], [23], [25], [32], [43], [44], has been addressed for years assuming that contact between the workpiece and tool is never lost. This gives a good representation of the reality for small changes in the cutting process parameters under steady-state conditions. However, modern

manufacturing requires a high flexibility of the cutting conditions and therefore a good understanding of the transients is essential to eliminate a catastrophic breakage of the tool. Despite the significant process made in perceiving the complex mechanism of the chip formation using linear models, a proper understanding will only be possible when the nonlinear nature of the chip-formation phenomena is unveiled and appropriately modelled. (Wiercigron[46]).

Recent investigations into nonlinear dynamics have shown an existence and importance of chaotic motion occurring in machining. The models by Grabec [10] and Wiercigroch [46] have shown evidence of chaotic vibrations, which occurs mainly due to the nonlinearity of dry friction and the intermittent contact between the cutting tool and the workpiece. In this thesis, the author uses the models by Grabec [10] and Wiercigroch [46] to explain the nonlinearity of the frictional and impact chatter in metal cutting processes. And in this thesis the metal cutting process based on the stochastic models was introduced to demonstrate the stochasticity of the cutting process instead of the deterministic models. With nonlinear dynamic analysis and simulations this model will demonstrate the frictional and impact chatter properly.

2.4.2 Chatter Suppression

Recent researches [5], [8], [9], [15], [21], [22], [37], [48], pay more and more attention to the active control of chatter. With the development of piezoelectric technology, piezoelectric actuators have become a standard option in positioning applications where the displacements must be small and highly accurate. In particular, ultra-precision manufacturing requires exceptionally fine and repeatable motions, making piezoelectric actuators a common choice. The research by Richter [34] shows the hysteretic behavior of piezoelectric actuator is a important problem for designing the control system. In this thesis, with the application of piezoelectric actuators in two directions x and y, we develop a adaptive controller to deal with unknown hysteresis. According to my knowledge there is no discussion in literature about frictional and impact chatter suppression by piezoelectric actuator. It is the first time that the frictional and impact chatter was combined with adaptive control system of nonlinear system with unknown hysteresis by using piezoelectric actuator. The simulation of the adaptive controller will show the suppression of frictional and impact chatter and stability of the metal cutting system.

Chapter 3

Dynamic Model of Piezoelectric Actuator

Piezoelectric actuators (piezo) are solid state (ceramic) actuators that convert electrical energy directly into motion (mechanical energy) of extremely high resolution.

Pierre and Jacques Curie [49]in 1880 were the first to experimentally demonstrate that there was a connection between macroscopic piezoelectric phenomena and crystallographic structure. Their experiment consisted of a conclusive measurement of surface charges appearing on specially prepared crystals (tourmaline, quartz, topaz, cane sugar and Rochelle salt among them) which were subjected to mechanical stress.

This effect was dubbed as "piezoelectricity".

The first serious applications of piezoelectric devices took place during World War I. In 1917, P. Langevin and French co-workers began to perfect an ultrasonic submarine detector [49]. Their transducer was a mosaic of thin quartz crystals glued between two steel plates (the composite having a resonant frequency of about 50 KHz), mounted in a housing suitable for submersion. Continuing their work after past the end of the war, they did achieve their goal of emitting a high frequency "chirp" underwater and measuring depth by timing the return echo. The strategic importance of their achievement was not overlooked by any industrial nation, and since that time the development of sonar transducers, circuits, systems, and materials have never ceased.

Now the commercial success of the Japanese efforts has attracted the attention of industry in many other nations and spurred a new effort to develop successful piezoceramic products. Another measure of activity is the rate and origin of article publications in the piezoelectric materials/applications area - there has been a large increase in publications rate in Russia, China and India.

3.1 Advantages of Piezoelectric Actuators

As a kind of new actuator, piezoelectric actuator has many advantages, such as:

- Sub-nanometer resolution
- Large force generation (> 10,000 N)
- Sub-millisecond response
- No magnetic fields
- Extremely low steady-state power consumption
- No wear and tear
- Vacuum and clean room compatibility
- Operation at cryogenic temperatures

3.1.1 Advantages of Piezoelectric Positioning Systems

Especially for positioning system, piezoelectric actuator shows lots of advantages.

- Unlimited Resolution

A piezoelectric actuator can produce extremely fine position changes down to the subnanometer range. The smallest changes in operating voltage are converted into smooth movements. Motion is not influenced by stiction/friction or threshold volt-

ages.

• Large Force Generation

Piezoelectric actuators can generate a force of several 10,000 N. Some units even can bear loads up to several tons and position within a range of more than 100 μm with subnanometer resolution.

• Fast Expansion

Piezoelectric actuators offer the fastest response time available (microsecond time constants). Acceleration rates of more than 10,000 g's can be obtained.

• No Magnetic Fields

The piezoelectric effect is related to electrical fields. Piezoelectric actuators do not produce magnetic fields nor are they affected by magnetic fields. They are specially well suited for applications where magnetic fields cannot be tolerated.

• Low Power Consumption

The piezoelectric effect directly converts electrical energy into motion only absorbing electrical energy during movement. Static operation, even holding heavy loads, does

not consume power.

• No Wear and Tear

A piezoelectric actuator has neither gears nor rotating shafts. Its displacement is based on solid state dynamics and shows no wear and tear.

• Vacuum and Clean Room Compatible

Piezoelectric actuators are ceramic elements that do not need any lubricants and show no wear and abrasion. This makes them clean room compatible and ideally suited for Ultra High Vacuum applications.

• Operation at Cryogenic Temperatures

The piezoelectric effect is based on electric fields and functions down to almost zero Kelvin.

3.2 Precision Positioning by Piezoelectric Actuators

3.2.1 Open and Closed Loop Operation

One essential feature of a piezoceramic actuator is its ability to make infinitely small movements, when a correspondingly small voltage signal is applied. This enables piezoelectric actuators for ultra precise positioning tasks (unlimited relative positioning sensitivity).

On the other hand, when a large change in the voltage signal is applied to a piezoelectric actuator, the actual position step width can be influenced by many internal and external parameters acting onto the actuator, so that in the first instant, the relationship between voltage and the induced motion can only roughly be predicted. This can be demonstrated by applying a series of random voltage steps to a piezoelectric actuator or by running a cycle over a distinct voltage range producing the well known hysteresis loop.

When a distinct piezoelectric voltage level is accessed from randomly distributed starting points of the actuator, the uncertainty in the final position is roughly equal

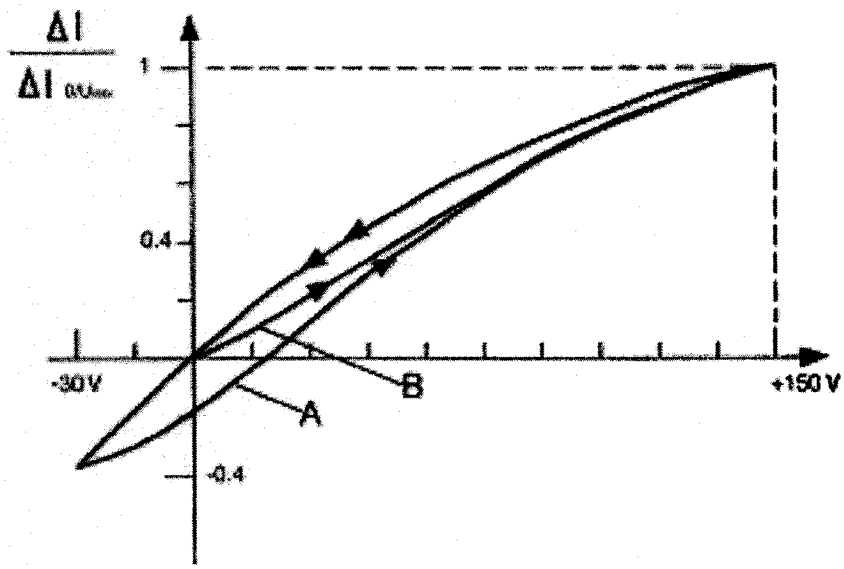

Figure 3.1: Open loop correlation of position and driving voltage [49]

to the intersection of the hysteresis field with the voltage level. So the uncertainty in open loop piezoelectric positioning in random access operation can be up to 10% to 15% of the actually applied total piezoelectric actuator range. In Figure 3.1 the characteristic of a low voltage actuator is shown for the full output voltage range -30 V to +150 V. Displacement hysteresis is about 15 % [49].

3.2.2 Basics of Closed Loop Operation

The actuator produces only a motion, but does not contain an inherent precise information about the exact position. To obtain this information of the actual position,

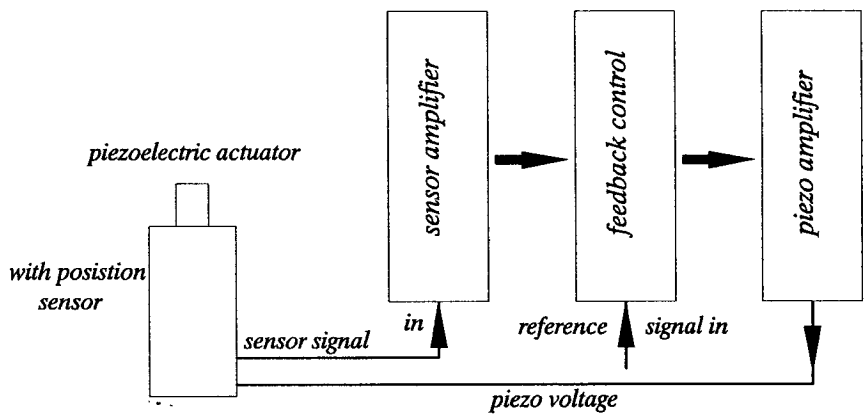

Figure 3.2: Model structure of the position control system feedback control unit

the actuator must be combined with a suitable kind of position sensitive sensor. "Suitable" means: sufficiently high in accuracy, repeatability and linearity.

By a feedback control logic, the real position of the actuator is permanently compared with the desired position, defined by the magnitude of the input signal. When there is a difference between wanted (reference) and real position, the feedback control drives the piezoelectric actuator to the perfect position and cancels the difference.

3.2.3 Piezoelectric Positioning System

The complete piezoelectric positioning system requires:

- the piezoelectric actuator including the position sensor option (strain gage),

• other electronic units (comprising all necessary modules, Figure 3.2) such as:

- sensor signal amplifying stage

- feedback control logic (including microprocessor)

- piezoelectric voltage amplifying unit

3.3 Piezoelectric System Companies

With the development of the piezoelectric system, more and more companies began to produce the piezoelectric system and do the researches.

• Piezo System Inc.

186 Massachusetts Avenue Cambridge,Massachusetts 02139 USA

Web: www.piezo.com

• Physik Instrumente (PI) GmbH Co. KG

Auf der Roerstrasse 1, D-76228 Karlsruhe/Palmbach, Germany

Web: www.physikinstrumente.de

• Piezomechanik GmbH

Berg am Laim Str. 64, D-81673 Munchen/Munich, Germany.

Web: www.piezomechanik.com

3.4 Technical Data of Piezoelectric Actuator

Here we choose the P-239 Piezoactuator as example to show the technical data and the limitation of the piezoactuator's motion.

Open-loop travel: 180 $\mu m \pm 20$ %

Close-loop travel $\geq$: 180 μm

Close-loop/open-loop resolution: 3.6/1.8 nm

Static large-signal stiffness: 35 $N/\mu m \pm 20\%$

Push/pull force capacity:4500/500 N

Torque limit(at tip): 1 Nm

Max. operation voltage: $-1000V$

Electrical capacitance: 2100 nF

Dynamic operating current coefficient: 17.5 $\mu A/(Hz \times \mu m)$

Unloaded resonant frequency: 2 kHz

Weight without cables: 400 g

3.5 Dynamic Model of Piezoelectric Actuator

Piezoelectric actuators have become a standard option in positioning applications where the displacements must be small and highly accurate. For the design of controller instead of using the traditional backlash hysteresis nonlinear model, a continuous-time dynamic model to describe a class of backlash-like hysteresis have been defined by Su *et. al.* [38]:

$$\frac{dw(t)}{dt} = \alpha \left| \frac{dv(t)}{dt} \right| (cv(t) - l(t)) + B\frac{dv(t)}{dt}, \tag{3.1}$$

where α, c, and B_1 are constants, satisfying $c > B_1$. And in Figure 3.3 the hysteresis curves given by equation (3.1) with $\alpha = 1$, $c = 3.1635$, and $B_1 = 0.345$ for $v(t) = k\ sin(2.3t)$ with $k = 2.5,\ 3.5,\ 4.5,\ 5.5$, and 6.5 was shown.

As the proof in [38], equation (3.1) can be solved explicitly for $v(t)$ piecewise monotone

$$w(t) = cv(t) + d(v(t)), \tag{3.2}$$

with

$$d(v(t)) = [w_0 - cv_0]e^{-\alpha(v-v_0)sgn(\dot{v})} + e^{-\alpha v sgn(\dot{v})} \int_{v_0}^{v} [B - c]e^{\alpha\zeta sgn(\dot{v})} d\zeta$$

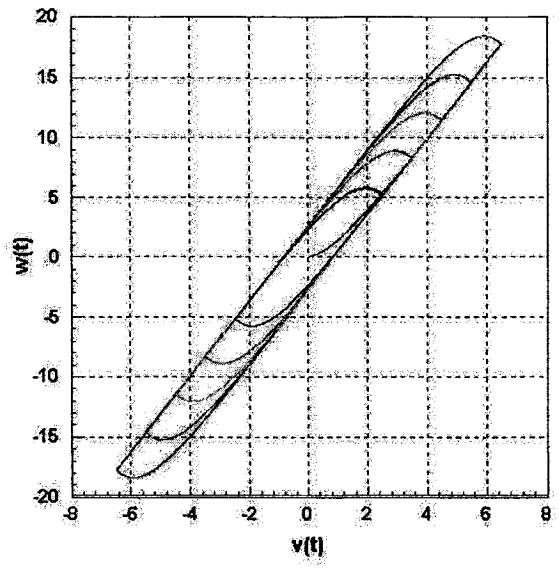

Figure 3.3: Hysteresis curves given by equation(3.1)[38]

As the proof in [38], it is important to note that there exists a uniform bound ρ such that

$$||d(v(t))|| \leq \rho \tag{3.3}$$

So the piezoelectric actuator force $f_p(v)$ can be described as

$$f_p = k_p[cv(t) + d(v(t))] \tag{3.4}$$

3.6 Application of Piezoelectric Actuator

The piezoelectric actuators are used as positioning device in the turning tool and is illustrated in Figure 3.3. The piezoelectric actuators can move the tool with high

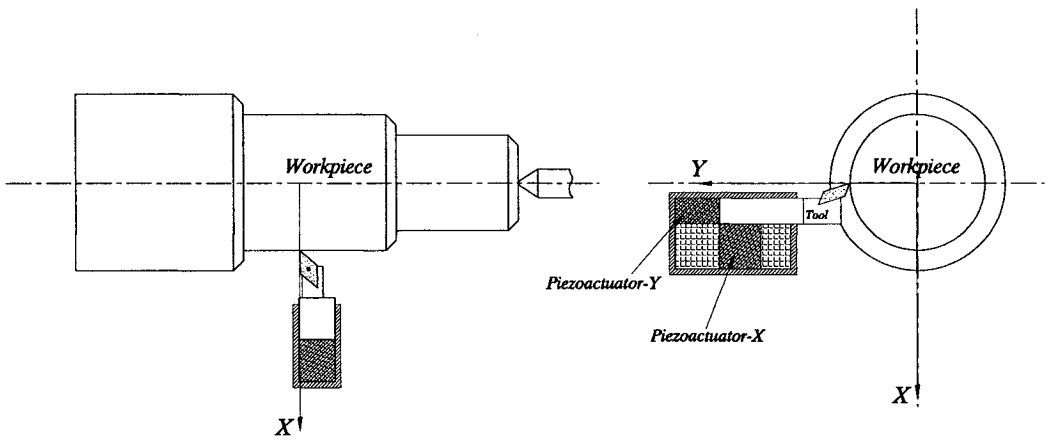

Figure 3.4: The scheme of turning tool with piezoelectric actuator

accuracy in two directions, X and Y. By applying the controlled electrical voltage, the piezoelectric actuators can expand as ordered in microseconds. With the expanding of the piezoelectric actuators, the cutting tool can be adjusted as commanded. Therefore the chatter can be overcome by the motion of piezoelectric actuators with the adaptive control system.

Chapter 4

Frictional and Impact Chatter in the Two-Degree-of-Freedom Deterministic Model

4.1 Dynamic Model

Dynamic interactions in any mechanical system may be described by the following second order differential equation [46].

$$\frac{d^2x}{dt^2} = f(t; x, \frac{dx}{dt}, p), \tag{4.1}$$

where $x(t)$ is the tool's displacement vector in x direction, p is the system-parameters vector and $f(\cdot)$ is the force vector, dependent on both the internal and external excitations.

The MT-CP system may be treated as a dynamic system with a feedback control, which is schematically depicted in Figure 4.1. During the chip formation, the vector of cutting force, f_{cut}, is generated and acts with the vector of other forces, f_o, on the machine tool structure. The require geometry, g_r, is distorted by the relative vibrations between the tool and the workpiece, which can be represented by the vector $(x, \dot{x})$.

We assume steady-state conditions and consider a three-dimensional vector of the cutting force, f_{cut}, which is dependent on the changes of the cutting parameters a_j, the process constant c_j and β_j, and the Heaviside function (Appendix B) $H_{j,l}$, to account for the separation between the tool and the workpiece. Thus the ith component of the cutting force can be evaluated from [46]

$$f_{cut,\,i} = \prod_{j=1}^{n} c_i a_j^{\beta_{i,j}} H_{j,\,l}(a_k), \qquad i = 1, 2, 3, \qquad l \in n, \qquad l \leq k < n. \tag{4.2}$$

where β is the collocation parameters, k is the time-step, and n is the period of one spindle revolution. The cutting parameters a_j are functions of the displacement and

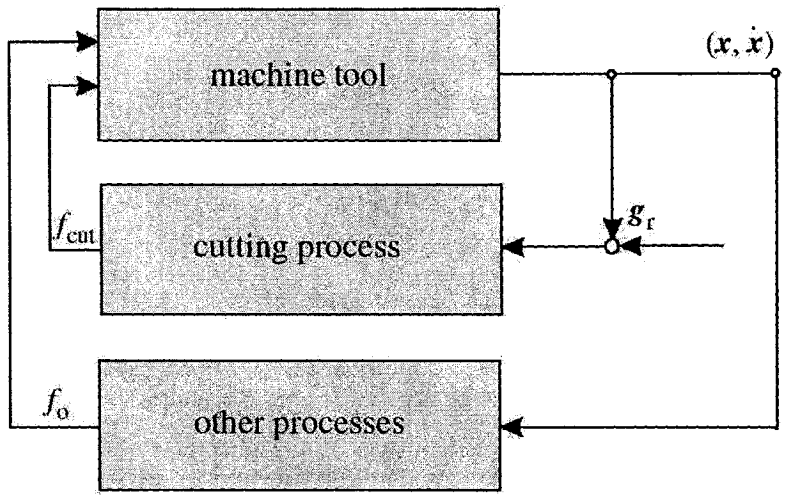

Figure 4.1: Dynamic interactions during a metal-cutting process

velocity, and can be written symbolically as follows:

$$a_j = g(x, \dot{x}), \tag{4.3}$$

4.2 Frictional and Impact Chatter in the Two-Degree-of-Freedom Deterministic Model

Because the instantaneous separation of the cutting tool from the workpiece has a great influence on the system dynamics, our model of the MT-CP system should take into account the feedback control loop through f_{cut}, and also the discontinuity of

the process. Illustrated in Figure 4.2 is a simple but realistic model of the MT-CP system under consideration. The elastic, dissipative and inertial properties of the machine-tool structure, tool and the workpiece are represented by a planar oscillator, which is excited by the cutting force components f_x and f_y. It is assumed that the relationship between the cutting forces and the chip geometry, namely the cutting process characteristics, is captured by orthogonal cutting, where the cutting edge is parallel to the workpiece and normal to the cutting direction, as depicted in Figure 4.2(b). In our case, the cutting parameter, a_j should be understood as the depth of the cut, h, and the relative velocity, v_r. Due to vibration in the x direction, the relative velocity v_r can cross the zero value point, therefore static and dynamic friction occurs. Thus the cutting process characteristics as a function of the relative velocity can not be expressed directly by the formulae (4.2) [46], therefore one can postulate the following relationships

$$f_x = h^{\beta_x} H(h) g_x(v_r), \tag{4.4}$$

$$f_y = h^{\beta_y} H(h) g_y(v_r), \tag{4.5}$$

Since f_x and f_y are mutually related, one can be expressed by the other. This approach was used by Hastings *et al.* [13], and the cutting forces formulas for a wide class of technical materials are provided [46]

$$f_x(y, x', y') = q_0 h(c_1(abs(v_r) - 1)^2 + 1)H(h), \tag{4.6}$$

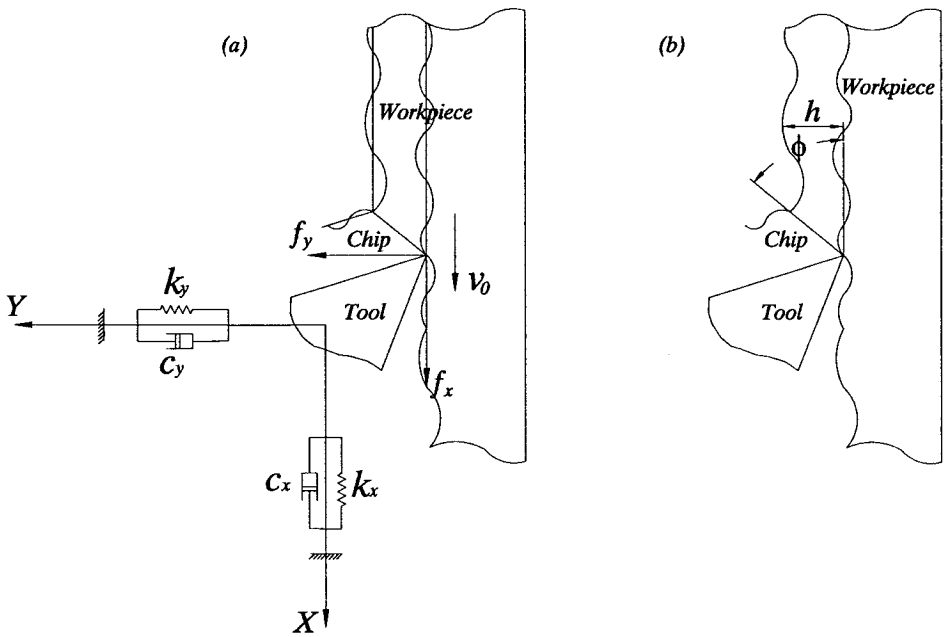

Figure 4.2: MT-CP system (a) physical model (b) chip geometry

$$f_y(y, x', y') = \chi(v_r, v_f, h) f_x(y, x', y'), \tag{4.7}$$

where

$\chi(\cdot) = (c_2(v_f - 1)^2 + 1)(c_3(h - 1)^2 + 1)H(f_x)sgn(v_f)$,

$v_r = v_0 - x'$

$v_f = v_0 - Ry'$,

$h = h_0 - y$,

$R = R_0(c_4(v_r - 1)^2 + 1)$,

where h is the depth of cut, v_r is the relative velocity, v_f is friction velocity, $\chi(\cdot)$ is the friction acting on the rake surface. $c_1 - c_4$ and q_0 are cutting parameters. R is the shear plastic deformation.

It is assumed that the force, f_y, is mainly due to the friction, $\chi(\cdot)$. The friction velocity, v_f, is reduced due to shear plastic deformation, R, which is represented by the shear angle, ϕ. [46]

$$R = ctg(\phi), \tag{4.8}$$

The cutting process starts with an initial depth of cut, h_0, where layers are taken out from the workpiece with the constant velocity, v_0. The rest of the cutting parameters $c_1 - c_4$ and q_0 are constants [46].

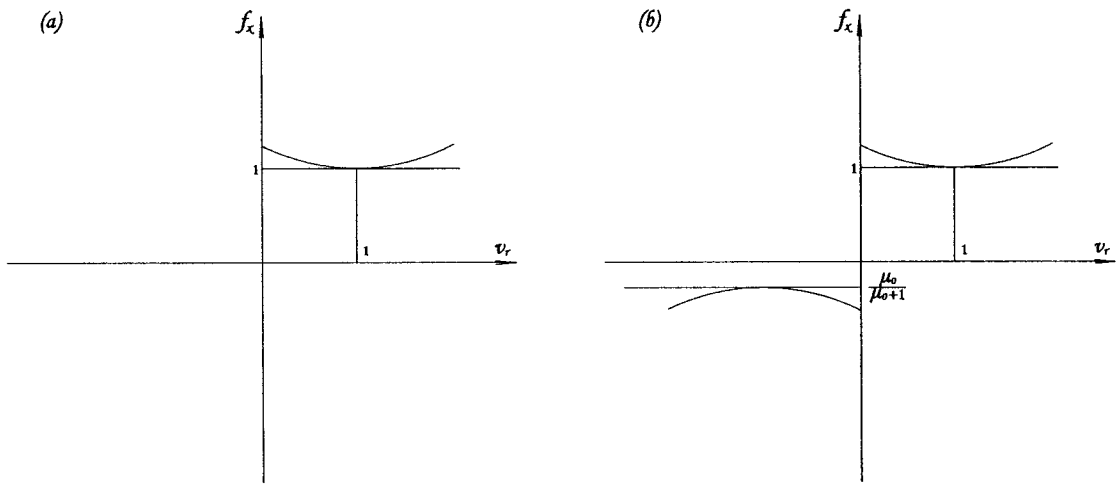

Figure 4.3: (a) Former form of f_x. (b) New form of f_x

Summarizing, the nonlinear relationship between the cutting force, f_x and chip velocity is graphically presented in Figure 4.3(a), where for $v_r < 0$ the excitation force is equal to zero. In reality this force never disappears as there is always a considerable friction force due to the compression force in the vertical spring. The outlined simplified approach can be found in the work by Grabec [10] and Wiercigroch [46]. To make it more realistic, a Coulomb friction force acting in the x direction for the $v_r < 0$ case needs to be added [46]. From the other hand, Equation (4.6) should be still valid to predict the total force, f_x for the $v_r \geq 0$ cases. A modified formulae, which satisfies the conditions listed above is written below presented graphically in

Figure 4.3(b)

$$f_x(y, x', y') = q_0 h \left(H(v_r) \frac{1}{1+\mu_0} + sgn(v_r) \frac{\mu_0}{1+\mu_0} \right) (c_1(abs(v_r) - 1)^2 + 1) H(h), \quad (4.9)$$

where μ_0 is a static friction coefficient.

And motion of the analyzed system can be described by a set of two second order differential equations, which are presented here in a non-dimensional form

$$x'' + 2\xi_x x' + x = f_x(y, x', y'), \quad (4.10)$$

$$y'' + 2\xi_y \sqrt{\alpha} y' + \alpha y = f_y(y, x', y'), \quad (4.11)$$

where

$\omega_{0x}^2 = \frac{c_x}{m}$,

$\omega_{0y}^2 = \frac{c_y}{m}$,

$\alpha = \frac{c_y}{c_x}$,

$\xi_x = \frac{k_x}{2m\omega_{0x}}$,

$\xi_y = \frac{k_y}{2m\omega_{0y}}$.

m is the mass of vibrating system, c_x, c_y are stiffness in x and y direction, k_x, k_y are viscous damping in x and y direction, ω_{0x}, ω_{0y} are natural frequency in x and y direction respectively, α is stiffness ratio, ξ_x, ξ_y are dimensionless coefficient of viscous

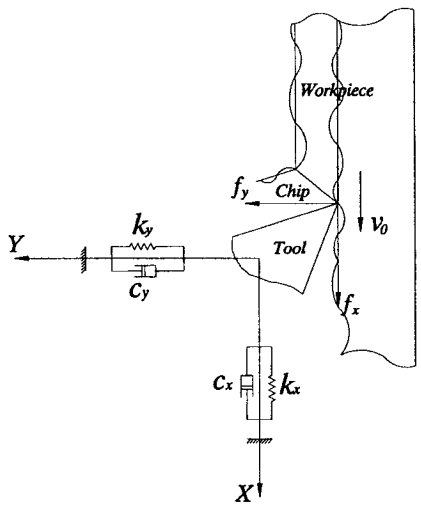

Figure 4.4: 2D model of orthogonal metal cutting

damping in the x and y direction respectively.

From Figure 4.4, the dynamic process of the metal cutting system can be described by a set of two second order differential equation.

$$\begin{bmatrix} 1 & 0 \\ 0 & 1 \end{bmatrix} \begin{bmatrix} x'' \\ y'' \end{bmatrix} + \begin{bmatrix} 2\xi_x & 0 \\ 0 & 2\xi_y\sqrt{\alpha} \end{bmatrix} \begin{bmatrix} x' \\ y' \end{bmatrix} + \begin{bmatrix} 1 & 0 \\ 0 & \alpha \end{bmatrix} \begin{bmatrix} x \\ y \end{bmatrix}$$
$$= \begin{bmatrix} 1 \\ \chi(v_r, v_f, h) \end{bmatrix} f_x(y, x', y') \tag{4.12}$$

where

$\chi(\cdot) = (c_2(v_f - 1)^2 + 1)(c_3(h-1)^2 + 1)H(f_x)sgn(v_f)$,

$\omega_{0x}^2 = \frac{c_x}{m}$,

$\omega_{0y}^2 = \frac{c_y}{m}$,

$\alpha = \frac{c_y}{c_x}$,

$\xi_x = \frac{k_x}{2m\omega_{0x}}$,

$\xi_y = \frac{k_y}{2m\omega_{0y}}$,

where $\chi(\cdot)$ is the friction acting on the rake surface. m is the mass of vibrating system, c_x, c_y are stiffness in x and y direction, k_x, k_y are viscous damping in x and y direction, ω_{0x}, ω_{0y} are natural frequency in x and y direction respectively, α is stiffness ratio, ξ_x, ξ_y are dimensionless coefficient of viscous damping in x and y direction respectively.

Then equation (4.12) can be written as:

$$\begin{aligned} x'' + 2\xi_x x' + x &= q_0(h_0 - y)\left(H(v_0 - x')\frac{1}{1+\mu_0} + sgn(v_0 - x')\frac{\mu_0}{1+\mu_0}\right) \\ &\quad \times\left(c_1\big(abs(v_0 - x') - 1\big)^2 + 1\right)H(h_0 - y), \end{aligned} \tag{4.13}$$

$$\begin{aligned} y'' + 2\xi_y\sqrt{\alpha}y' + \alpha y &= \Big(c_2(v_0 - Ry' - 1)^2 + 1\Big)\Big(c_3(h_0 - y - 1)^2 + 1\Big)H(f_x) \\ &\quad \times\left(H(v_0 - x')\frac{1}{1+\mu_0} + sgn(v_0 - x')\frac{\mu_0}{1+\mu_0}\right) \end{aligned}$$

$$\times\left(c_1\Big(abs(v_0 - x') - 1\Big)^2 + 1\right)H(h_0 - y)$$
$$\times sgn(v_0 - Ry')q_0(h_0 - y), \tag{4.14}$$

4.3 Simulation of the Deterministic Model

Figures 4.5 (a) and (b) (J.Warminski et al. [42]) show plots of initial velocity v_0 as a functions of cutting force magnitude, q_0, and initial depth of cut, h_0, with the upper solid line delineating the theoretically stable region (white) from the theoretically unstable region (grey). The dotted line is the corresponding numerical solution for the upper solid line. Numerical simulations were carried out by means of the fourth order Runge-Kutta method, and vibrations of the system were analyzed for small initial conditions. The dotted line in the figures divides the parameter plane into two regions with a stable regime predicted for the space above the line and unstable behavior below.

Illustrated in Figure 4.5 (a) (Plot of feed velocity v_0 as a function of the magnitude of the cutting force q_0) the multiple scales analysis (analytical result AR-solid curve) and numerical analysis based on the original equations of the motion due to Wiercigroch [46] (numerical solution NS-dotted curve). Stable area is white, unstable area

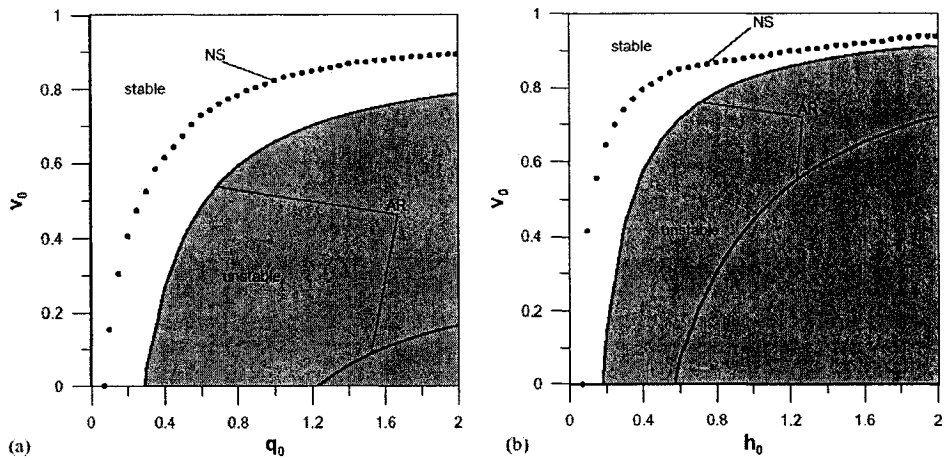

Figure 4.5: (a) Plot of v_0 as a function of q_0. (b)Plot of v_0 as a function of h_0.[42]

is grey. Additional data is, $\mu_0 = 0.1$, $c_1 = 0.3$, $c_2 = 0.7$, $c_3 = 1.5$, $c_4 = 1.2$, $h_0 = 0.5$, $R_0 = 2.2$, $\alpha = 4$, $\xi_x = 0.1$, $\xi_y = 0.1$.

Illustrated in Figure 4.5 (b) (Plot of feed velocity v_0 as a function of the initial depth of cut h_0) the multiple scales analysis (analytical result AR-solid curve) and numerical analysis based on the original equations of motion due to Wiercigroch [46] (numerical solution NS-dotted curve). Stable area is white, unstable area is grey. Additional data is $\mu_0 = 0.1$, $c_1 = 0.3$, $c_2 = 0.7$, $c_3 = 1.5$, $c_4 = 1.2$, $R_0 = 2.2$, $\alpha = 4$, $\xi_x = 0.1$, $\xi_y = 0.1$.

As the analyzed system is nonlinear and can exhibit a broad range of responses, it

is essential to provide a high-accuracy integration routine. Each time a discontinuity occurs, the precise value of the time has to be calculated in order to provide the correct initial conditions for the next integration step. For a given set of parameters and initial condition, the numerical integration is carried out using the fourth-order Runge-Kutta procedure with a fixed time-step, $\Delta t = 0.001s$, until a discontinuity is detected. Figure 4.6 to Figure 4.11 show the simulation results for the 2D deterministic model in stable region and unstable region. Illustrated in Figures 4.6, 4.7 and 4.8, when the $h = 0.5$, $q_0 = 1.2$, $v_0 = 0.4$ and $\Delta t = 0.001s$ in unstable region as shown in Figure 4.5, the chatter occurs. Not only the x vibrates, but also the x'changes along with time. The relation between x and x' clearly shows that this is not stable. Similar as what we just saw, for y, y', f_x, f_y and h, they all have the similar results. Additional data is $\mu_0 = 0.1$, $c_1 = 0.3$, $c_2 = 0.7$, $c_3 = 1.5$, $c_4 = 1.2$, $R_0 = 2.2$, $\alpha = 4$, $\xi_x = 0.1$, $\xi_y = 0.1$. The system shows vibrations in both directions x (Figure 4.6(a) and 4.6(b)) and y (Figure 4.7(d) and 4.7(e)), which is confirmed by the phase plane portraits (Figure 4.6 (c) and 4.7(f)).

Illustrated in Figures 4.9, 4.10 and 4.11, when the $h = 0.5$, $q_0 = 1.2$, $v_0 = 0.8$ and $\Delta\tau = 0.001s$ in stable region as shown in Figure 4.5, the chatter can not be hold in stable region. Additional data is $\mu_0 = 0.1$, $c_1 = 0.3$, $c_2 = 0.7$, $c_3 = 1.5$, $c_4 = 1.2$,

$R_0 = 2.2$, $\alpha = 4$, $\xi_x = 0.1$, $\xi_y = 0.1$. It is clearly that the cutting system response is decreasing rapidly onto equilibrium state of the system in both directions x (Figure 4.9(a) and 4.9(b)) and y (Figure 4.10(d) and 4.10(e)), which is confirmed by the phase plane portraits (Figure 4.9 (c) and 4.10(f)).

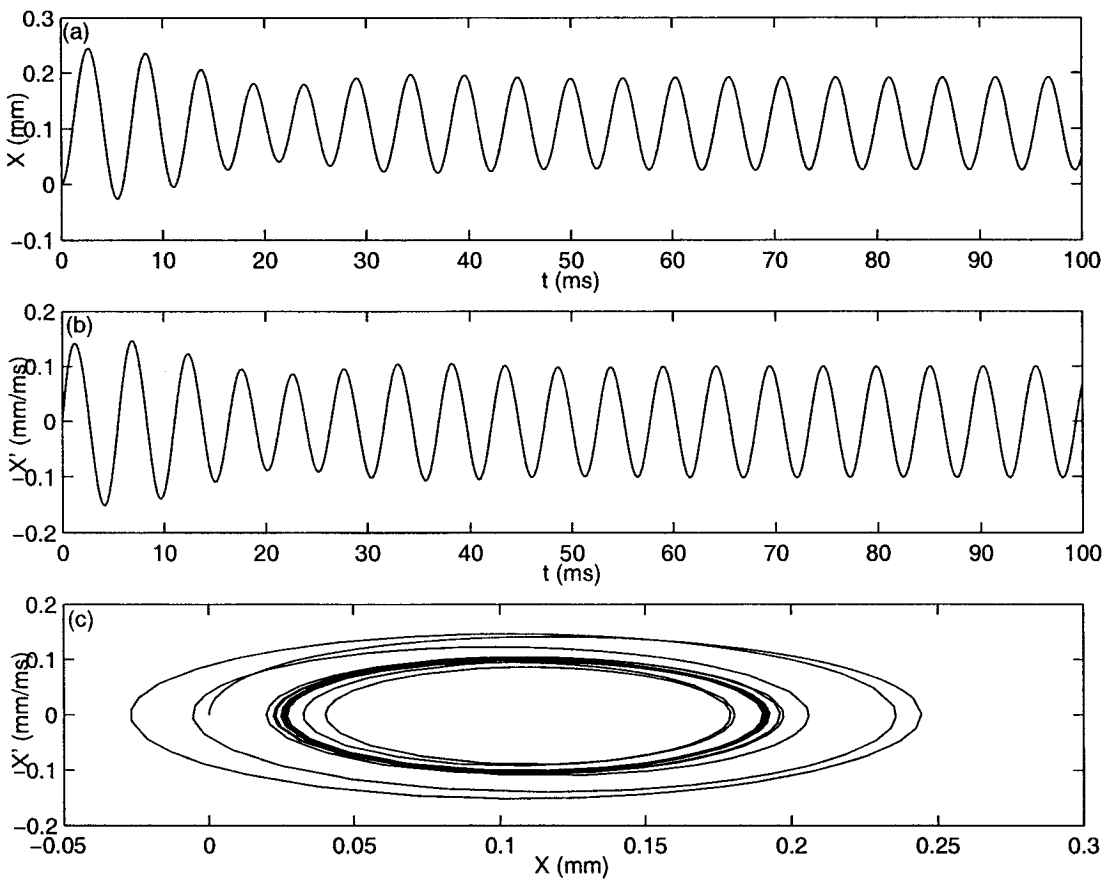

Figure 4.6: x and x' for the system in unstable region

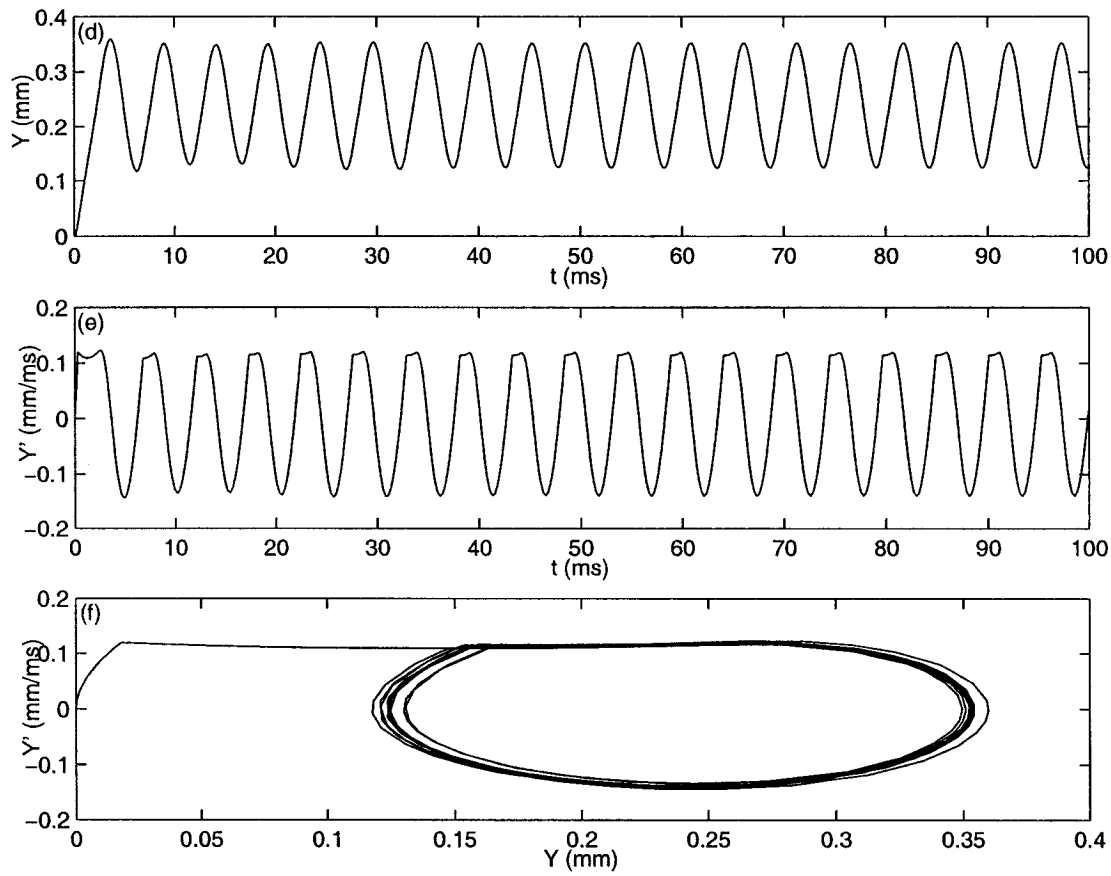

Figure 4.7: y and y' for the system in unstable region

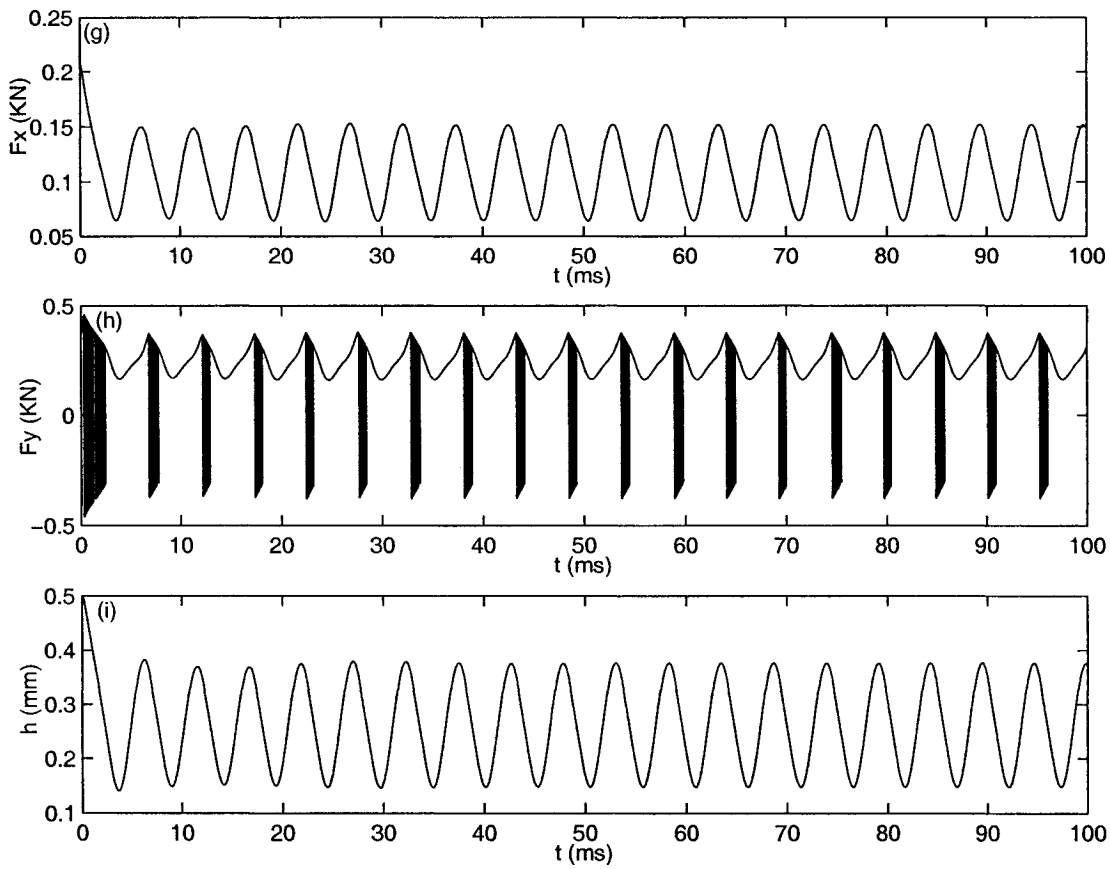

Figure 4.8: F_x F_y and h for the system in unstable region

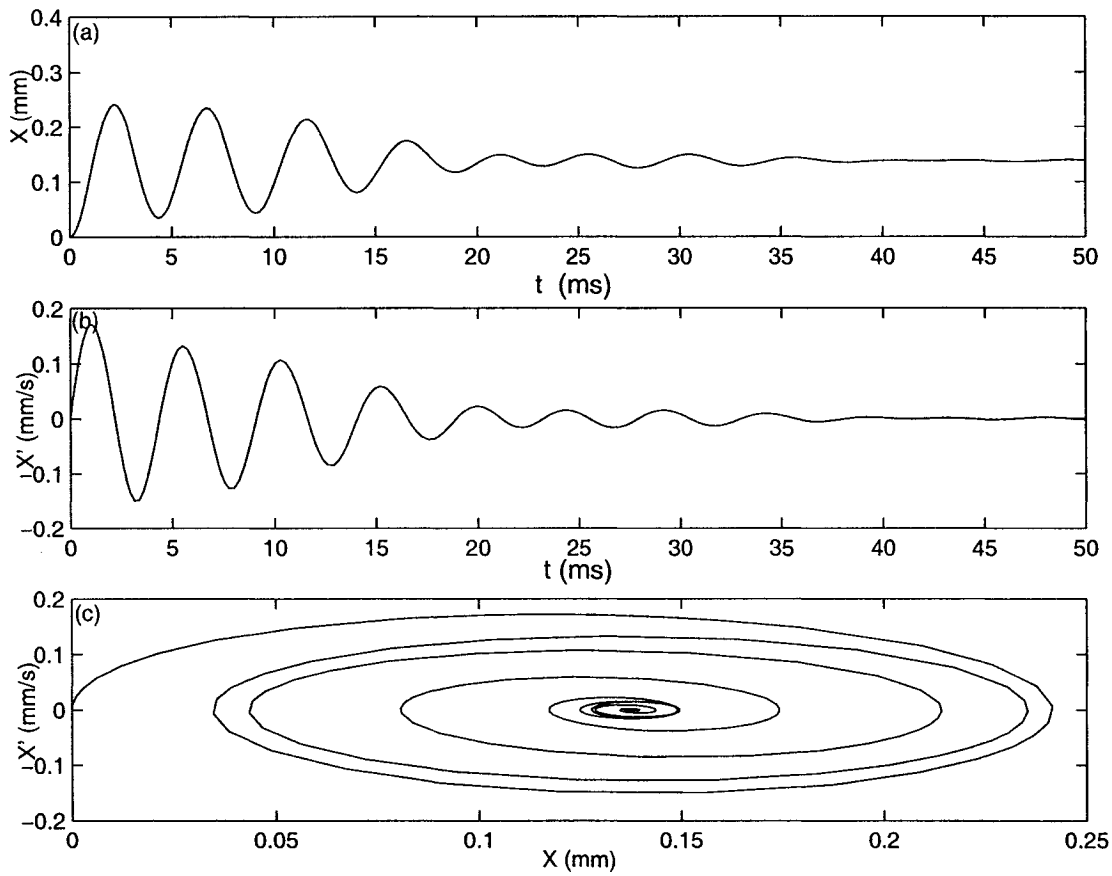

Figure 4.9: x and x' for the system in stable region

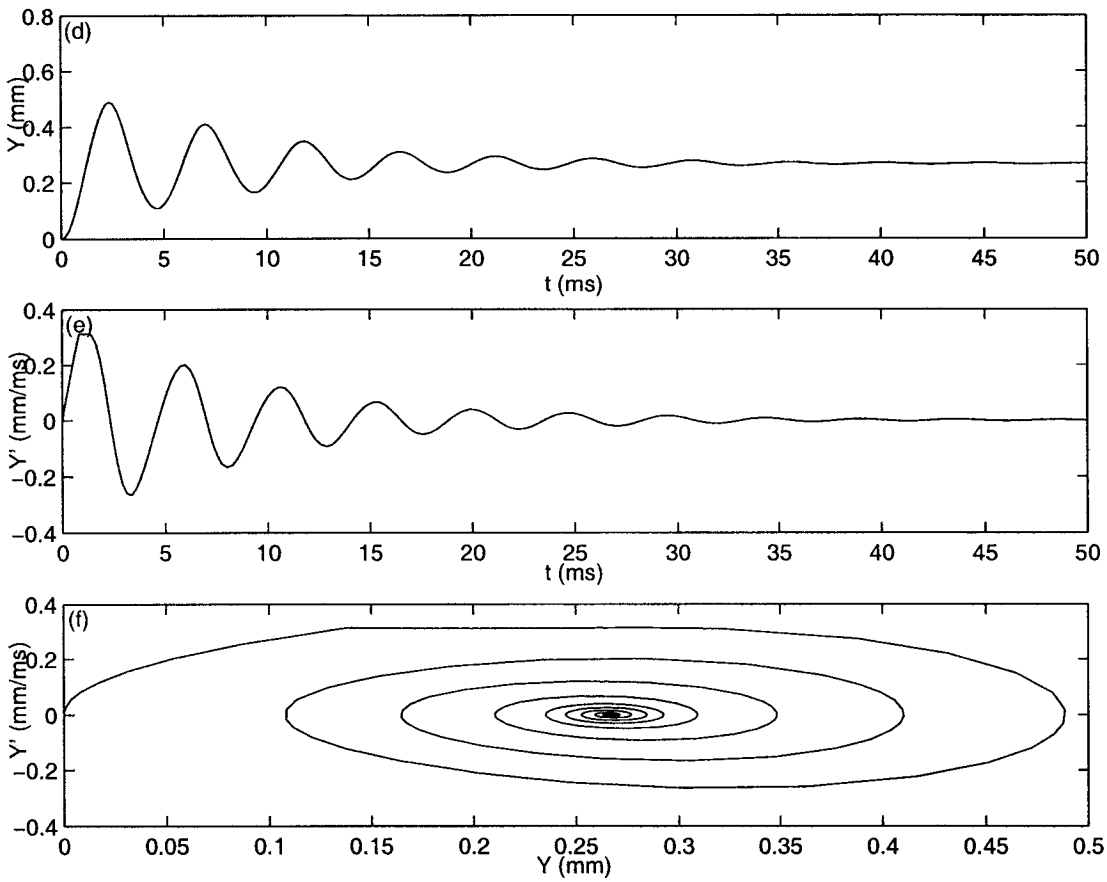

Figure 4.10: y and y' for the system in stable region

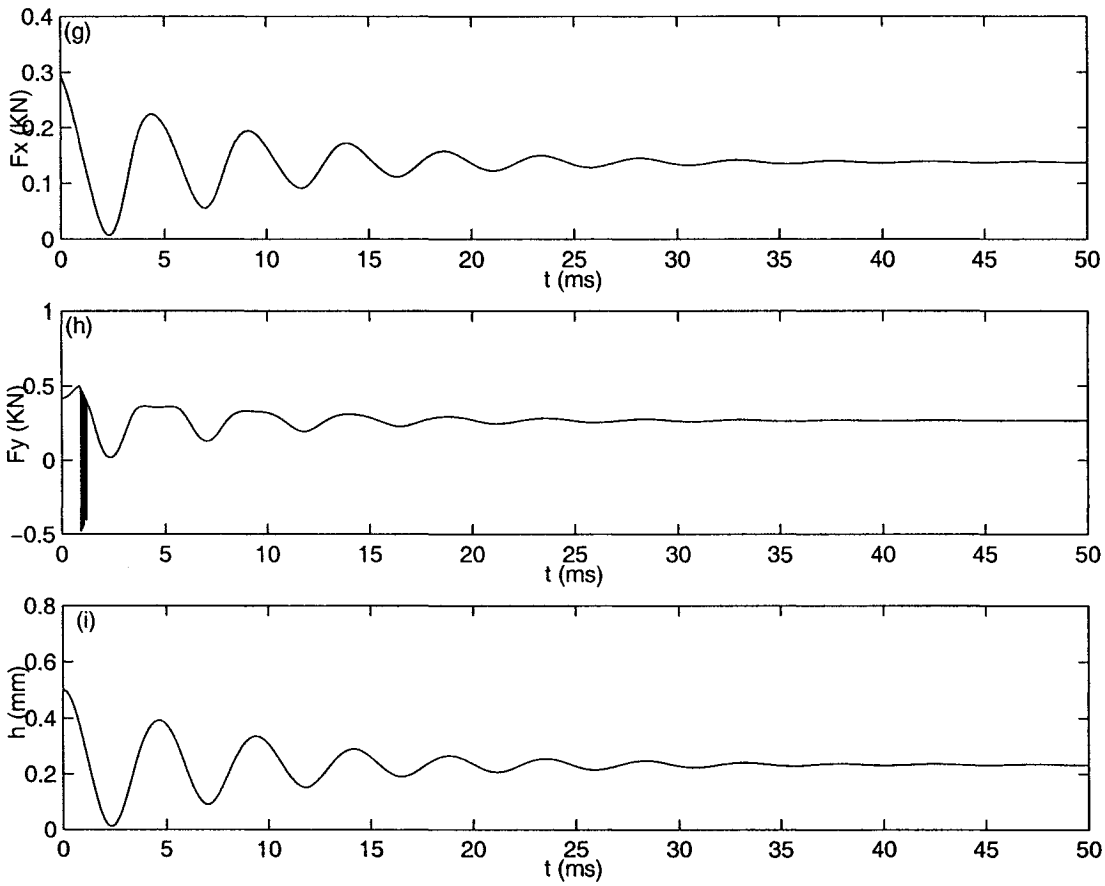

Figure 4.11: F_x F_y and h for the system in stable region

Chapter 5

Active Control for Chatter with 2-D Deterministic Model and Piezoelectric Actuator

This chapter considers the suppression for the chatter in metal cutting system by use of piezoelectric actuators. The 2D deterministic model of the metal cutting system is modelled in Figure 5.1. The robust adaptive control laws of nonlinear system with hysteresis by Su *et. al.* [38] are used in the suppression of chatter because of the hysteresis of the piezoelectric actuator. The simulation of the responses of the control system will show the result of the adaptive control laws.

5.1 System Dynamic Model

Illustrated in Figure 5.1 a simple but realistic model of the MT-CP system that is being considered. The elastic, dissipative and inertia properties of the machine-tool structure, tool and the workpiece are represented by a planar oscillator, which is excited by the cutting force components f_x and f_y. It is assumed that the relationship between the cutting forces and the chip geometry, namely the cutting process characteristics, is captured by orthogonal cutting, where the cutting edge is parallel to the workpiece and normal to the cutting direction, as depicted in Figure 5.1(b). And two piezoelectric actuators are in the direction X and Y. From Figure 5.1, the dynamic process of the metal cutting system can be described by a set of two second order differential equation.

$$\begin{bmatrix} 1 & 0 \\ 0 & 1 \end{bmatrix} \begin{bmatrix} x'' \\ y'' \end{bmatrix} + \begin{bmatrix} 2\xi_x & 0 \\ 0 & 2\xi_y\sqrt{\alpha} \end{bmatrix} \begin{bmatrix} x' \\ y' \end{bmatrix} + \begin{bmatrix} 1 & 0 \\ 0 & \alpha \end{bmatrix} \begin{bmatrix} x \\ y \end{bmatrix}$$
$$= \begin{bmatrix} 1 \\ \chi(v_r, v_f, h) \end{bmatrix} f_x(y, x', y') + \begin{bmatrix} 1 & 0 \\ 0 & 1 \end{bmatrix} \begin{bmatrix} f_{px} \\ f_{py} \end{bmatrix} \tag{5.1}$$

$$f_{px} = k_{mpx}[cu_x(t) + d\big(u_x(t)\big)] \tag{5.2}$$

$$f_{py} = k_{mpy}[cu_y(t) + d\big(u_y(t)\big)] \tag{5.3}$$

$$f_x(y, x', y') = q_0 h(c_1(abs(v_r) - 1)^2 + 1)H(h), \tag{5.4}$$

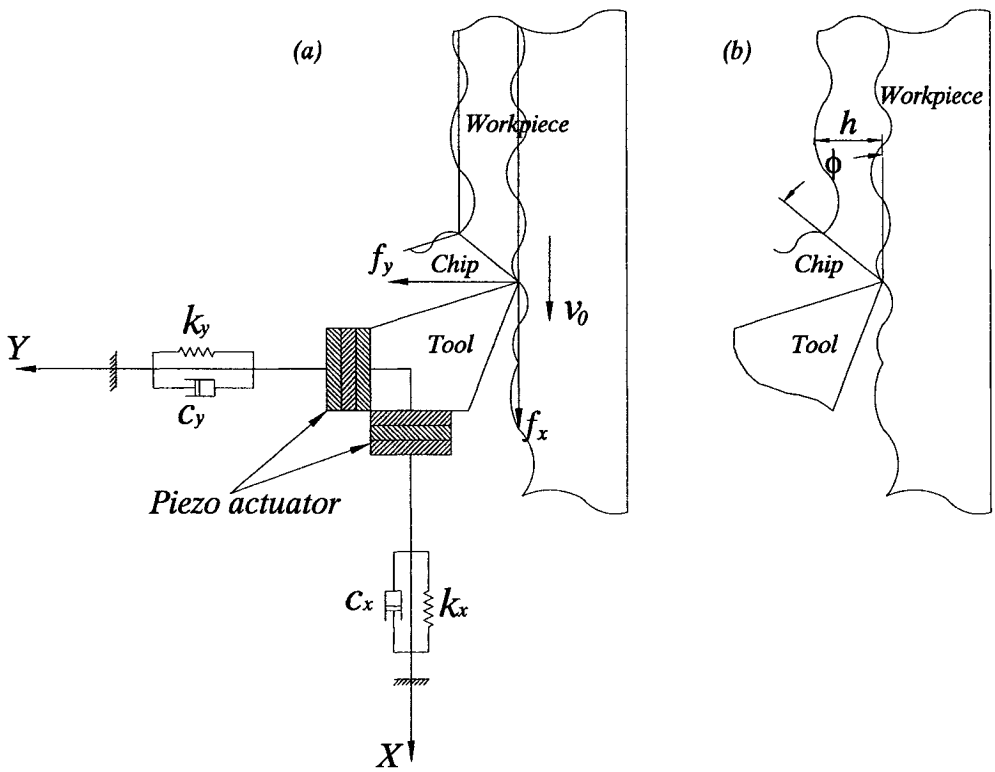

Figure 5.1: Model of cutting system with two piezoelectric actuators

$$f_y(y, x', y') = \chi(v_r, v_f, h) f_x(y, x', y'), \tag{5.5}$$

where

$\chi(\cdot) = (c_2(v_f - 1)^2 + 1)(c_3(h-1)^2 + 1)H(f_x)sgn(v_f)$,

$v_r = v_0 - x'$

$v_f = v_0 - Ry'$,

$h = h_0 - y$,

$R = R_0(c_4(v_r - 1)^2 + 1)$,

$\omega_{0x}^2 = \frac{c_x}{m}$,

$\omega_{0y}^2 = \frac{c_y}{m}$,

$\alpha = \frac{c_y}{c_x}$,

$\xi_x = \frac{k_x}{2m\omega_{0x}}$,

$\xi_y = \frac{k_y}{2m\omega_{0y}}$,

$k_{mpx} = \frac{k_{px}}{m}$,

$k_{mpy} = \frac{k_{py}}{m}$,

where h is the depth of cut, v_r is the relative velocity, v_f is friction velocity, $\chi(\cdot)$ is the friction acting on the rake surface. $c_1 - c_4$ and q_0 are cutting parameters. R is shear plastic deformation. m is the mass of vibrating system, c_x, c_y are stiffness in x and y direction, k_x, k_y are viscous damping in x and y direction, ω_{0x}, ω_{0y} are natural frequency in x and y direction respectively, α is stiffness ratio, ξ_x, ξ_y are dimensionless

coefficient of viscous damping in x and y direction respectively. $\chi(\cdot)$ is the friction acting on the rake surface. f_{px} and f_{py} are the forces of the piezoelectric actuators in x and y.

The cutting process starts with an initial depth of cut, h_0, where layers are taken out from the workpiece with the constant velocity, v_0. The rest of the cutting parameters $c_1 - c_4$ and q_0 are constants.

5.2 Adaptive Controller Design

The closed-loop dynamic system of metal cutting system in turning with piezoelectric actuators and adaptive controllers is illustrated in Figure 5.2.

Equation (5.1) can be transformed as follows:

$$\begin{aligned} x'' + 2\xi_x x' + x &= q_0(h_0 - y)\left(H(v_0 - x')\frac{1}{1+\mu_0} + sgn(v_0 - x')\frac{\mu_0}{1+\mu_0}\right) \\ &\quad \times\left(c_1\big(abs(v_0 - x') - 1\big)^2 + 1\right)H(h_0 - y) + f_{px}, \end{aligned} \tag{5.6}$$

$$\begin{aligned} y'' + 2\xi_y\sqrt{\alpha}y' + \alpha y &= \Big(c_2(v_0 - Ry' - 1)^2 + 1\Big)\Big(c_3(h_0 - y - 1)^2 + 1\Big)H(f_x) \\ &\quad \times\left(H(v_0 - x')\frac{1}{1+\mu_0} + sgn(v_0 - x')\frac{\mu_0}{1+\mu_0}\right) \end{aligned}$$

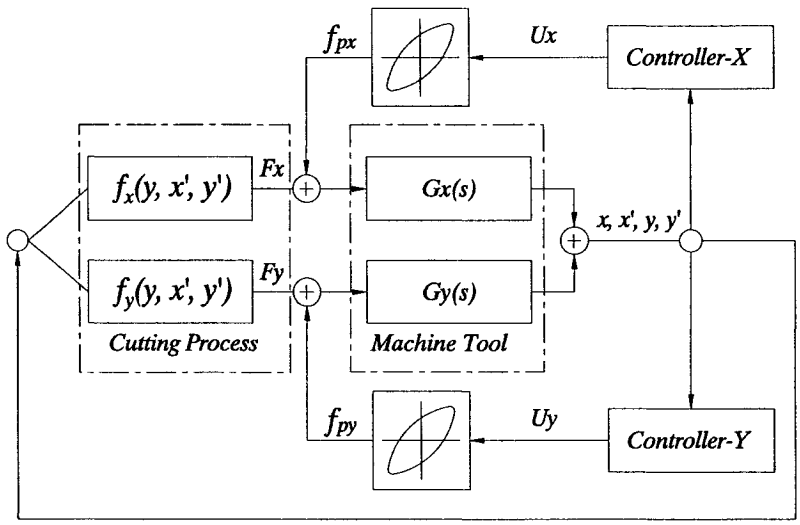

Figure 5.2: Block diagram of turning system with piezoelectric actuators

$$\times\left(c_1\left(abs(v_0 - x') - 1\right)^2 + 1\right)H(h_0 - y)$$
$$\times sgn(v_0 - Ry')q_0(h_0 - y) + f_{py}, \tag{5.7}$$

A filtered tracking error is defined as

$$\delta(t) = \begin{bmatrix} \delta_1(t) \\ \\ \delta_2(t) \end{bmatrix} = \begin{bmatrix} x(t) + \lambda_1 x'(t) \\ \\ y(t) + \lambda_2 y'(t) \end{bmatrix} = 0 \tag{5.8}$$

A turning error δ_ϵ, as follows:

$$\delta_{i\epsilon} = \delta_i - \epsilon\ sat\left(\frac{\delta_i}{\epsilon}\right) \quad i = 1, 2 \tag{5.9}$$

where ϵ is an arbitrary positive constant and $sat(\cdot)$ is the saturation function (Appendix C).

Differentiating $\delta(t)$ with respect to time t as:

So

$$\begin{aligned}\dot{\delta_1}(t) &= (1-2\lambda_1\xi_x)x' - \lambda_1 x + \lambda_1 q_0(h_0-y) \\ &\times\left(H(v_0-x')\frac{1}{1+\mu_0} + sgn(v_0-x')\frac{\mu_0}{1+\mu_0}\right) \\ &\times\left(c_1\Big(abs(v_0-x')-1\Big)^2+1\right)H(h_0-y) \\ &+\lambda_1 k_{mpx}[cu_x(t) + d_x\Big(u_x(t)\Big)],\end{aligned} \tag{5.10}$$

$$\begin{aligned}\dot{\delta_2}(t) &= (1-2\lambda_2\xi_y\sqrt{\alpha})y' - \lambda_2\alpha y + \lambda_2(c_2(v_0-Ry'-1)^2+1) \\ &\times(c_3(h_0-y-1)^2+1)H(f_x)sgn(v_0-Ry')q_0(h_0-y) \\ &\times\left(H(v_0-x')\frac{1}{1+\mu_0} + sgn(v_0-x')\frac{\mu_0}{1+\mu_0}\right) \\ &\times(c_1(abs(v_0-x')-1)^2+1)H(h_0-y) \\ &+\lambda_2 k_{mpy}[cu_y(t) + d_y\Big(u_y(t)\Big)],\end{aligned} \tag{5.11}$$

The above can be simplified:

$$\dot{\delta_1}(t) = \lambda_{x1}x' - \lambda_{x2}x + \eta_x(y)\varsigma_x(x') + \lambda_{x3}u_x(t) + \lambda_{x4}d_x\Big(u_x(t)\Big) \tag{5.12}$$

$$\dot{\delta_2}(t) = \lambda_{y1}y' - \lambda_{y2}y + \eta_y(y)\varsigma_y(x') + \lambda_{y3}u_y(t) + \lambda_{y4}d_y\Big(u_y(t)\Big), \tag{5.13}$$

where

$$\eta_x(y) = \lambda_1 q_0(h_0 - y)H(h_0 - y)$$

$$\varsigma_x(x') = \left(H(v_0 - x')\frac{1}{1+\mu_0} + sgn(v_0 - x')\frac{\mu_0}{1+\mu_0}\right)\left(c_1\Big(abs(v_0 - x') - 1\Big)^2 + 1\right)$$

$$\eta_y(y) = \lambda_2(c_2(v_0 - Ry' - 1)^2 + 1)(c_3(h_0 - y - 1)^2 + 1)sgn(v_0 - Ry')q_0(h_0 - y)H(h_0 - y)$$

$$\varsigma_y(x') = H(f_x)\left(H(v_0 - x')\frac{1}{1+\mu_0} + sgn(v_0 - x')\frac{\mu_0}{1+\mu_0}\right)(c_1(abs(v_0 - x') - 1)^2 + 1)$$

$$\lambda_{x1} = (1 - 2\lambda_1\xi_x),\ \ \lambda_{x2} = \lambda_1,\ \ \lambda_{x3} = \lambda_1 k_{mpx}c,\ \ \lambda_{x4} = \lambda_1 k_{mpx},$$

$$\lambda_{y1} = 1 - 2\lambda_2\xi_y\sqrt{\alpha},\ \ \lambda_{y2} = \lambda_2\alpha,\ \ \lambda_{y3} = \lambda_2 k_{mpy}c,\ \ \lambda_{y4} = \lambda_2 k_{mpy}$$

Then define

$$\theta_{x1} = \frac{\lambda_{x1}}{\lambda_{x3}},\ \theta_{x2} = \frac{\lambda_{x2}}{\lambda_{x3}},\ \theta_{x3} = \frac{1}{\lambda_{x3}},\ \theta_{x4} = \frac{\lambda_{x4}}{\lambda_{x3}}.$$

$$\theta_{y1} = \frac{\lambda_{y1}}{\lambda_{y3}},\ \theta_{y2} = \frac{\lambda_{y2}}{\lambda_{y3}},\ \theta_{y3} = \frac{1}{\lambda_{y3}},\ \theta_{x4} = \frac{\lambda_{y4}}{\lambda_{y3}}.$$

The following control and adaptation laws are presented:

$$u_x(t) = -\left[k_{x\tau}\delta_1(t) + \hat{\theta}_{x1}x'(t) + \hat{\theta}_{x2}x(t) + \hat{\theta}_{x3}\psi_x(t) + k_x^* sat(\frac{\delta_1(t)}{\epsilon})\right] \tag{5.14}$$

$$u_y(t) = -\left[k_{y\tau}\delta_2(t) + \hat{\theta}_{y1}y'(t) + \hat{\theta}_{y2}y(t) + \hat{\theta}_{y3}\psi_y(t) + k_y^* sat(\frac{\delta_2(t)}{\epsilon})\right] \tag{5.15}$$

$$\psi_x(t) = \eta_x(y)\varsigma_x(x') \tag{5.16}$$

$$\psi_y(t) = \eta_y(y)\varsigma_y(x') \tag{5.17}$$

$$\dot{\hat{\theta}}_{xi} = proj(\hat{\theta}_{xi},\ -\gamma_{xi}\vartheta_{xi}) \tag{5.18}$$

$$\dot{\hat{\theta}}_{yi} = proj(\hat{\theta}_{yi},\ -\gamma_{yi}\vartheta_{yi}) \tag{5.19}$$

where $k_{x\tau}$ and $k_{y\tau}$ are constant positive gains, and k_x^* and k_y^* are control gains, satisfying $k_x^* \geq \rho/c_{min}$ and $k_y^* \geq \rho/c_{min}$, whereby, ρ is defined in Equation (2.3). The parameter γ_{xi} and γ_{yi} are positive constants determining the rates of adaptations, the $proj(\cdot,\cdot)$ is a projection operator, which is formulated as follows [38]:

$$proj(\hat{\theta}_{xi},\ -\gamma_{xi}\vartheta_{xi}) = \begin{cases} 0 & : \ if\ \hat{\theta}_{xi} = \theta_{ximax}\ and\ \gamma_{xi}\vartheta_{xi} < 0 \\ -\gamma_{xi}\vartheta_{xi} & : \ if\ [\theta_{ximin} < \hat{\theta}_{xi} < \theta_{ximax}] \\ & : \ or[\hat{\theta}_{xi} = \theta_{ximax}\ and\ \gamma_{xi}\vartheta_{xi} \geq 0] \\ & : \ or\ [\hat{\theta}_{xi} = \theta_{ximin}\ and\ -\gamma_{xi}\vartheta_{xi} \leq 0] \\ 0 & : \ if\ \hat{\theta}_{xi} = \theta_{ximin}\ and\ \gamma_{xi}\vartheta_{xi} > 0 \end{cases} \tag{5.20}$$

where

$\vartheta(t)_{x1} = \delta_{1\epsilon}(t)x'(t)$,

$\vartheta(t)_{x2} = \delta_{1\epsilon}(t)x(t)$,

$\vartheta(t)_{x3} = \delta_{1\epsilon}(t)\psi_x(t)$.

and

$$proj(\hat{\theta}_{yi},\ -\gamma_{yi}\vartheta_{yi}) = \begin{cases} 0 & : \ if\ \hat{\theta}_{yi} = \theta_{yimax}\ and\ \gamma_{yi}\vartheta_{yi} < 0 \\ -\gamma_{yi}\vartheta_{yi} & : \ if\ [\theta_{yimin} < \hat{\theta}_{yi} < \theta_{yimax}] \\ & : \ or[\hat{\theta}_{yi} = \theta_{yimax}\ and\ \gamma_{yi}\vartheta_{yi} \geq 0] \\ & : \ or\ [\hat{\theta}_{yi} = \theta_{yimin}\ and\ -\gamma_{yi}\vartheta_{yi} \leq 0] \\ 0 & : \ if\ \hat{\theta}_{yi} = \theta_{yimin}\ and\ \gamma_{yi}\vartheta_{yi} > 0 \end{cases} \tag{5.21}$$

where

$\vartheta(t)_{y1} = \delta_{2\epsilon}(t)y'(t)$,

$\vartheta(t)_{y2} = \delta_{2\epsilon}(t)y(t)$,

$\vartheta(t)_{y3} = \delta_{2\epsilon}(t)\psi_y(t)$.

5.2.1 Stability Analysis of the System

To establish global boundedness, we define a Lyapunov function candidate :

$$V(t) = \frac{1}{2}\left[\frac{1}{\lambda_{x3}}\delta_{1\epsilon}^2 + \frac{1}{\lambda_{y3}}\delta_{2\epsilon}^2 + \sum_{i=1}^{3}[\frac{1}{\gamma_{xi}}(\hat{\theta}_{xi}(t) - \theta_{xi})^2] + \sum_{i=1}^{3}[\frac{1}{\gamma_{yi}}(\hat{\theta}_{yi}(t) - \theta_{yi})^2]\right] \tag{5.22}$$

i) Since the discontinuity at $|\delta(t)| = \epsilon$ is of the first kind and since $\delta_{i\epsilon}(t) = 0$ when $|\delta(t)| \leq \epsilon$, it follows that the derivative $\dot{V}(t)$ exists for all $\delta(t)$, which is

$$\dot{V}(t) = 0 \quad when\ |\delta(t)| \leq \epsilon. \tag{5.23}$$

ii) When $|\delta(t)| > \epsilon$, using Equation (5.16) and the fact $\delta_{i\epsilon}\dot{\delta}_{i\epsilon} = \delta_{i\epsilon}\dot{\delta}_i$, one has

$$\begin{aligned}
\dot{V}(t) &= \frac{1}{\lambda_{x3}}\delta_{1\epsilon}\dot{\delta}_1 + \sum_{i=1}^{3}[\frac{1}{\gamma_{xi}}(\hat{\theta}_{xi}(t) - \theta_{xi})\dot{\hat{\theta}}_{xi}(t)] \\
&\quad + \frac{1}{\lambda_{y3}}\delta_{2\epsilon}\dot{\delta}_2 + \sum_{i=1}^{3}[\frac{1}{\gamma_{yi}}(\hat{\theta}_{yi}(t) - \theta_{yi})\dot{\hat{\theta}}_{yi}(t)] \\
&= \delta_{1\epsilon}[\theta_{x1}x'(t) + \theta_{x2}x(t) + \theta_{x3}\psi_x(t) + u_x(t) + \theta_{x4}d\Big(u_x(t)\Big)] \\
&\quad + \sum_{i=1}^{3}[\frac{1}{\gamma_{xi}}(\hat{\theta}_{xi}(t) - \theta_{xi})\dot{\hat{\theta}}_{xi}(t)] \\
&\quad + \delta_{2\epsilon}[\theta_{y1}y'(t) + \theta_{y2}y(t) + \theta_{y3}\psi_y(t) + u_y(t) + \theta_{y4}d\Big(u_y(t)\Big)] \\
&\quad + \sum_{i=1}^{3}[\frac{1}{\gamma_{yi}}(\hat{\theta}_{yi}(t) - \theta_{yi})\dot{\hat{\theta}}_{yi}(t)] \\
&= \delta_{1\epsilon}[\theta_{x1}x'(t) + \theta_{x2}x(t) + \theta_{x3}\psi_x(t) + \theta_{x4}d\Big(u_x(t)\Big)] \\
&\quad + \sum_{i=1}^{3}[\frac{1}{\gamma_{xi}}(\hat{\theta}_{xi}(t) - \theta_{xi})\dot{\hat{\theta}}_{xi}(t)] \\
&\quad - \delta_{1\epsilon}\left[k_{x7}\delta_1(t) + \hat{\theta}_{x1}x'(t) + \hat{\theta}_{x2}x(t) + \hat{\theta}_{x3}\psi_x(t) + k_x^* sat(\frac{\delta_1(t)}{\epsilon})\right] \\
&\quad + \delta_{2\epsilon}[\theta_{y1}y'(t) + \theta_{y2}y(t) + \theta_{y3}\psi_y(t) + \theta_{y4}d\Big(u_y(t)\Big)] \\
&\quad + \sum_{i=1}^{3}[\frac{1}{\gamma_{yi}}(\hat{\theta}_{yi}(t) - \theta_{yi})\dot{\hat{\theta}}_{yi}(t)] \\
&\quad - \delta_{2\epsilon}\left[k_{y7}\delta_2(t) + \hat{\theta}_{y1}y'(t) + \hat{\theta}_{y2}y(t) + \hat{\theta}_{y3}\psi_y(t) + k_y^* sat(\frac{\delta_2(t)}{\epsilon})\right] \qquad (5.24)
\end{aligned}$$

The above equation can be simplified, by the choice of $\delta_{i\epsilon}$, as

$$\begin{aligned}
\dot{V}(t) &\leq \delta_{1\epsilon}[\theta_{x1}x'(t) + \theta_{x2}x(t) + \theta_{x3}\psi_x(t) + \theta_{x4}d\Big(u_x(t)\Big)] \\
&\quad + \sum_{i=1}^{3}[\frac{1}{\gamma_{xi}}(\hat{\theta}_{xi}(t) - \theta_{xi})\dot{\hat{\theta}}_{xi}(t)]
\end{aligned}$$

$$
\begin{aligned}
&-k_{x\tau}\delta_{1\epsilon}^2 - \delta_{1\epsilon}\left[\hat{\theta}_{x1}x'(t) + \hat{\theta}_{x2}x(t) + \hat{\theta}_{x3}\psi_x(t) + k_x^* sat(\frac{\delta_1(t)}{\epsilon})\right] \\
&+\delta_{2\epsilon}[\theta_{y1}y'(t) + \theta_{y2}y(t) + \theta_{y3}\psi_y(t) + \theta_{y4}d\big(u_y(t)\big)] \\
&+\sum_{i=1}^{3}[\frac{1}{\gamma_{yi}}(\hat{\theta}_{yi}(t) - \theta_{yi})\dot{\hat{\theta}}_{yi}(t)] \\
&-k_{y\tau}\delta_{2\epsilon}^2 - \delta_{2\epsilon}\left[\hat{\theta}_{y1}y'(t) + \hat{\theta}_{y2}y(t) + \hat{\theta}_{y3}\psi_y(t) + k_y^* sat(\frac{\delta_2(t)}{\epsilon})\right] \qquad (5.25)
\end{aligned}
$$

By using adaptive laws (5.17), and the properties:

$$\frac{1}{\gamma_{xi}}(\hat{\theta}_{xi} - \theta_{xi})Proj(\hat{\theta}_{xi},\ -\gamma_{xi}\vartheta_{xi}) \leq (\hat{\theta}_{xi} - \theta_{xi})\vartheta_{xi}$$

$$\frac{1}{\gamma_{yi}}(\hat{\theta}_{yi} - \theta_{yi})Proj(\hat{\theta}_{yi},\ -\gamma_{yi}\vartheta_{yi}) \leq (\hat{\theta}_{yi} - \theta_{yi})\vartheta_{yi}$$

one obtains

$$
\begin{aligned}
\dot{V}(t) \ \leq\ & \delta_{1\epsilon}\left[\theta_{x1}x'(t) + \theta_{x2}x(t) + \theta_{x3}\psi_x(t) + \theta_{x4}d\big(u_x(t)\big)\right] \\
&+(\hat{\theta}_{x1} - \theta_{x1})\delta_{1\epsilon}x'(t) + (\hat{\theta}_{x2} - \theta_{x2})\delta_{1\epsilon}x(t) + (\hat{\theta}_{x3} - \theta_{x3})\delta_{1\epsilon}\psi_x(t) \\
&-k_{x\tau}\delta_{1\epsilon}^2 - \delta_{1\epsilon}\left[\hat{\theta}_{x1}x'(t) + \hat{\theta}_{x2}x(t) + \hat{\theta}_{x3}\psi_x(t) + k_x^* sat(\frac{\delta_1(t)}{\epsilon})\right] \\
&+\delta_{2\epsilon}\left[\theta_{y1}y'(t) + \theta_{y2}y(t) + \theta_{y3}\psi_y(t) + \theta_{y4}d\big(u_y(t)\big)\right] \\
&+(\hat{\theta}_{y1} - \theta_{y1})\delta_{2\epsilon}y'(t) + (\hat{\theta}_{y2} - \theta_{y2})\delta_{2\epsilon}y(t) + (\hat{\theta}_{y3} - \theta_{y3})\delta_{2\epsilon}\psi_y(t) \\
&-k_{y\tau}\delta_{2\epsilon}^2 - \delta_{2\epsilon}\left[\hat{\theta}_{y1}y'(t) + \hat{\theta}_{y2}y(t) + \hat{\theta}_{y3}\psi_y(t) + k_y^* sat(\frac{\delta_2(t)}{\epsilon})\right] \\
=\ & -k_{x\tau}\delta_{1\epsilon}^2 - k_x^*\delta_{1\epsilon}sat(\frac{\delta_1(t)}{\epsilon}) + \theta_{x4}\delta_{1\epsilon}d\big(u_x(t)\big) \\
&-k_{y\tau}\delta_{2\epsilon}^2 - k_y^*\delta_{2\epsilon}sat(\frac{\delta_2(t)}{\epsilon}) + \theta_{y4}\delta_{2\epsilon}d\big(u_y(t)\big) \qquad (5.26)
\end{aligned}
$$

Since $|\delta_{i\epsilon}| = \delta_{i\epsilon} sat(\frac{\delta_i}{\epsilon})$ for $|\delta_i| > \epsilon$, $||d(u_x(t))|| \leq \rho$ and $||d(u_y(t))|| \leq \rho$ the above becomes

$$\begin{aligned} \dot{V}(t) &\leq -k_{x\tau}\delta_{1\epsilon}^2 - k_x^*|\delta_{1\epsilon}| + \theta_{x4} d\Big(u_x(t)\Big)|\delta_{1\epsilon}| \\ &\quad -k_{x\tau}\delta_{1\epsilon}^2 - k_x^*|\delta_{1\epsilon}| + \theta_{x4} d\Big(u_x(t)\Big)|\delta_{1\epsilon}| \end{aligned} \tag{5.27}$$

Then we define $k_x^* = k_{xmax}^* \geq \rho\theta_{xmax}$ and $k_y^* = k_{ymax}^* \geq \rho\theta_{ymax}$ we will get

$$\begin{aligned} \dot{V}(t) &\leq -k_{x\tau}\delta_{1\epsilon}^2 - k_x^*|\delta_{1\epsilon}| + \theta_{x4} d\Big(u_x(t)\Big)|\delta_{1\epsilon}| \\ &\quad -k_{x\tau}\delta_{1\epsilon}^2 - k_x^*|\delta_{1\epsilon}| + \theta_{x4} d\Big(u_x(t)\Big)|\delta_{1\epsilon}| \\ &\leq -k_{x\tau}\delta_{1\epsilon}^2 - k_{y\tau}\delta_{2\epsilon}^2 \end{aligned} \tag{5.28}$$

5.2.2 Simulation of the Dynamic System

To suppress the chatter the adaptive control law (Equation 5.17) is introduced into the system (Equation 5.1). The parameters limits are $\theta_{x1} \in [-4.5e(-4), -2.5e(-4)]$, $\theta_{x2} \in [3.5e(-4), 2.0e(-4)]$, $\theta_{x3} \in [-4.2e(-4), -2.2e(-4)]$, $\theta_{x4} \in [5.0e(-4), 1.5e(-3)]$, $\theta_{y1} \in [-5.5e(-4), -3.5e(-4)]$, $\theta_{y2} \in [4.0e(-4), 6.5e(-4)]$, $\theta_{y3} \in [-5.5e(-4), -2.5e(-4)]$, $\theta_{y4} \in [5.0e(-4), 1.5e(-3)]$. Then we are taking initial data as $\theta_{x1} = -3.85e(-4)$, $\theta_{x2} = 1.4e(-4)$, $\theta_{x3} = -3.57e(-4)$, $\theta_{x4} = 1.0e(-3)$, $\theta_{y1} = -4.9e(-4)$, $\theta_{y2} = 5.7e(-4)$, $\theta_{y3} = -4.3e(-4)$, $\theta_{y4} = 1.0e(-3)$, $\gamma_{xi} = 1$ $(i = 1, 2, 3)$, $\gamma_{yi} = 1$ $(i = 1, 2, 3)$, $\epsilon = 1.0e(-4)$ and $K_\tau = 2.0e(-4)$. For a given set of parameters and initial condition, the

numerical integration is carried out using the fourth-order Runge-Kutta procedure with a fixed time-step, $\Delta t = 0.001s$. Figure 5.2 to Figure 5.5 show the simulation results for the chatter suppression in 2D deterministic model when $h = 0.5$, $q_0 = 1.2$, $v_0 = 0.4$. Additional data is $\mu_0 = 0.1$, $c_1 = 0.3$, $c_2 = 0.7$, $c_3 = 1.5$, $c_4 = 1.2$, $R_0 = 2.2$, $\alpha = 4$, $\xi_x = 0.1$, $\xi_y = 0.1$, $h = 0.5$, $q_0 = 1.2$, $v_0 = 0.4$ and $\Delta\tau = 0.001s$ (The same data as we have shown in charter 4 , unstable region). It is clear that the adaptive controller suppress the chatter and makes the cutting force being stable. In Figure 5.2 the x and x' will be stable due to the adjustment by piezoelectric actuator in 5 millisecond . In Figure 5.3 the y and y' will be stable due to the adjustment by piezoelectric actuator. In Figure 5.4 the F_x F_y and h will be stable due to the adjustment by piezoelectric actuator. Finally the U_x and U_y were shown in Figure 5.5.

5.3 Summary

In this chapter the adaptive control law for the deterministic model was developed. The stability of the cutting system was examined and the simulation results show that the piezoelectric actuators in x and y directions with the adaptive control law suppress the frictional and impact chatter successfully.

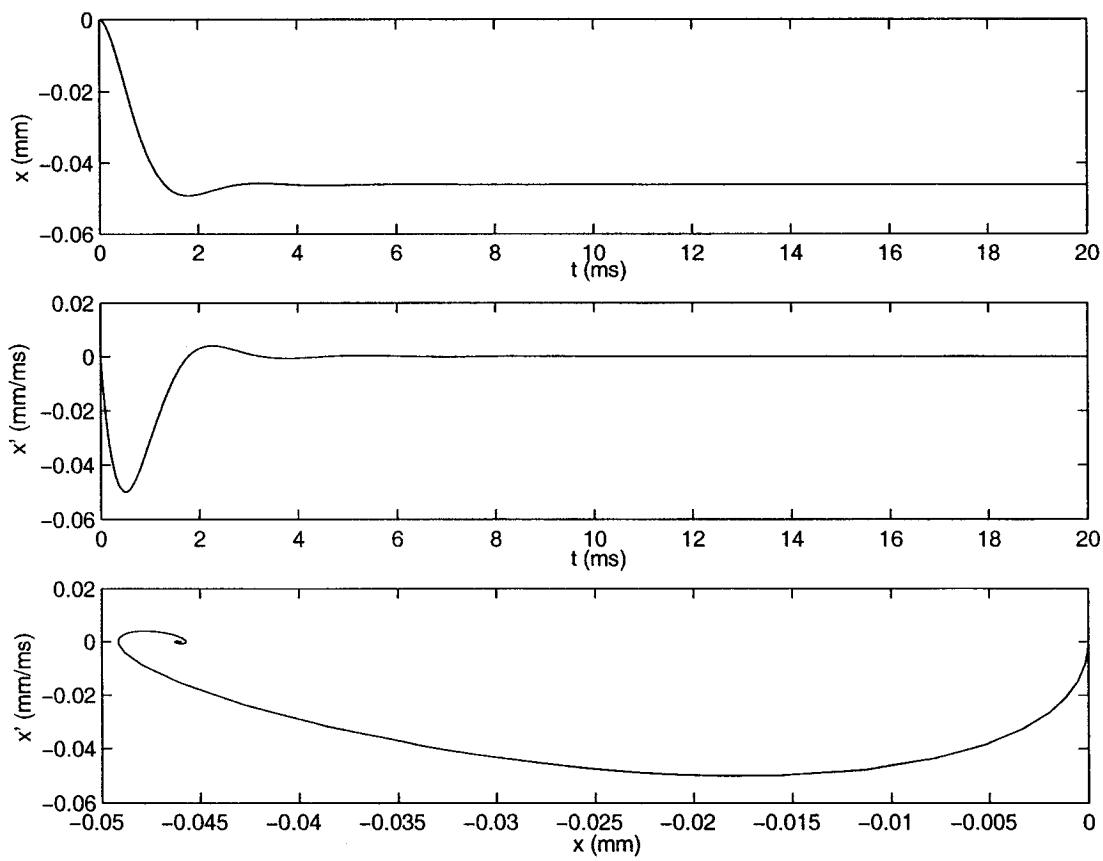

Figure 5.3: x and x' of the adaptive control system

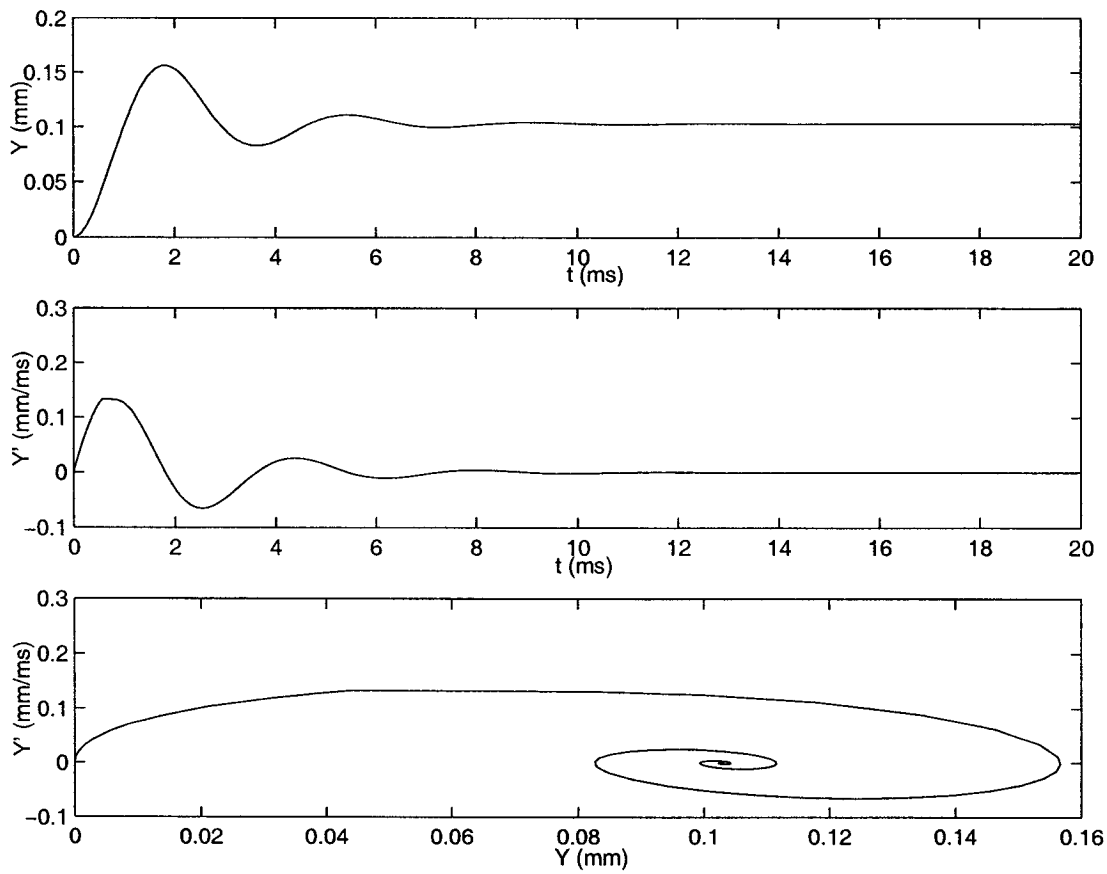

Figure 5.4: y and y' of the adaptive control system

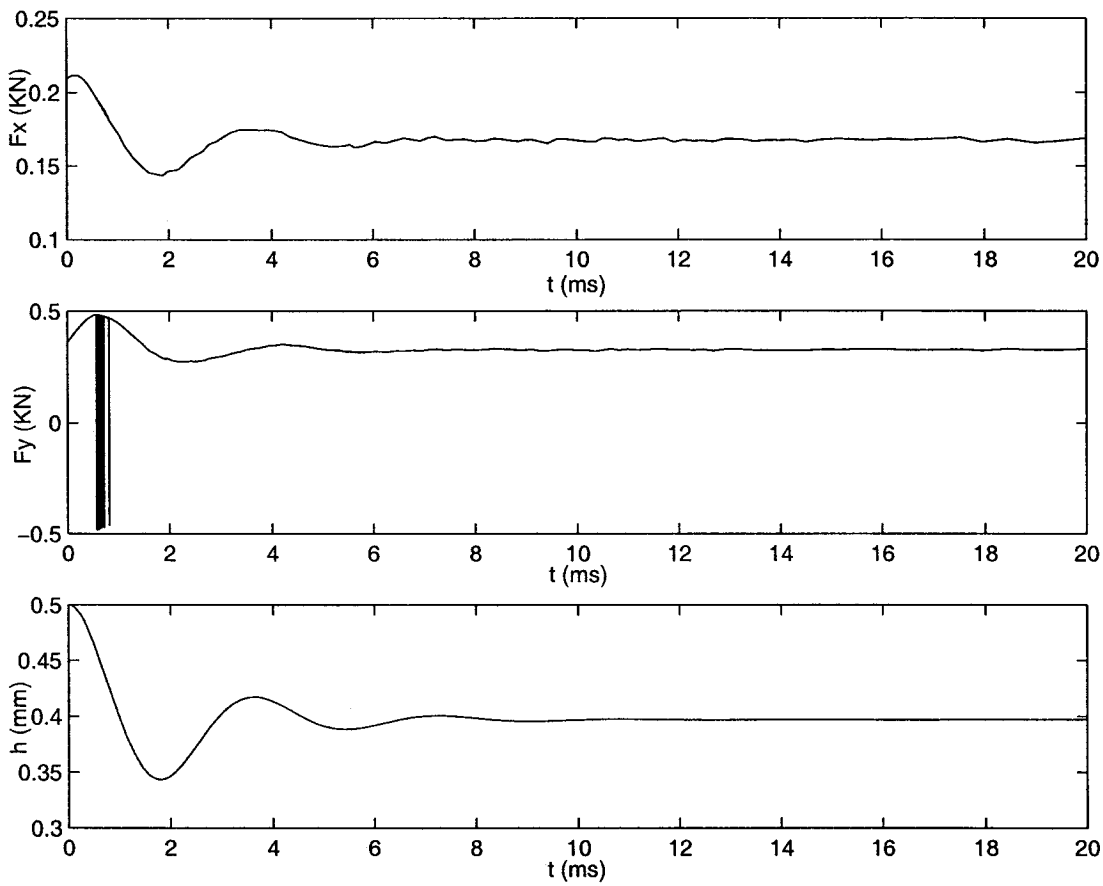

Figure 5.5: F_x, F_y, and h of the adaptive control system

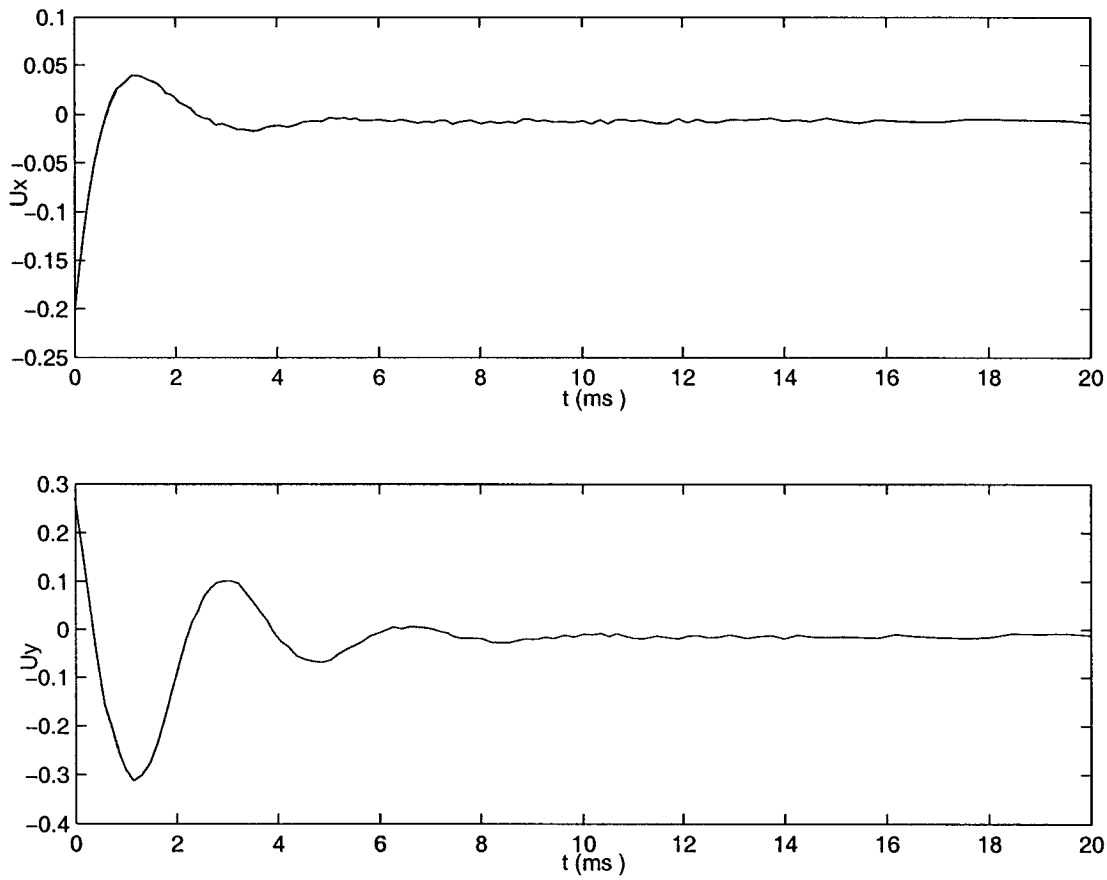

Figure 5.6: U_x and U_y of the adaptive control system

Chapter 6

Frictional and Impact Chatter in the Two-Degree-of-Freedom Stochastic Model

6.1 Two-Degree-of-Freedom Stochastic Model

When a workpiece is being turned on a lathe, the chatter irregularity will cause an inhomogeneity which leads to a random cutting resistance. Though considerable progress in the modelling of dynamic interactions occurring during metal cutting has been made, the models are mostly deterministic, using average values of the cutting-

material coefficients, and do not take into account the stochastic issues. For sure, the randomness of the cutting resistance is worth examining because of the varying grain size of the workpiece. There is a random cutting resistance because of the chip irregularities. A rigorous mathematical treatment of the plastic deformation for inhomogeneous material is a complex issue and so far no solid foundation has been laid in this area. As a consequence, a simplified but pragmatic approach is used to model the cutting resistance. This can be expressed as a function of the cutting-tool trajectory, and takes the form (Wiercigroch & Cheng [45]),

$$c(r) = c(x, y, z,) \tag{6.1}$$

where $r(t) = (x(t), y(t), z(t))$ is a parametric function of time. In this thesis we consider the cutting resistance as a one-dimensional process, which is a reasonable approximation for orthogonal cutting. It is assumed that the cutting resistance has been normalized by its mean so that the mean value $\bar{c}$ is equal to 1,

$$\lim_{l\to\infty} \frac{1}{l} \int_0^l c(x)\, dx = 1 \tag{6.2}$$

where l is a reference length of cut, and $c(x)$ is the specific (normalized) cutting resistance. Subtracting the mean value from $c(x)$, we obtain the fluctuation quantity $\hat{c}(x) = c(x) - \bar{c}$, where $\hat{c}$ is a zero-mean one-dimensional univariate weakly stationary

Ganssian process. It is characterized by a standard deviation η, and an autocorrelation coefficient $R(z)$, where z is the distance separating two points. A power spectral density function $S(\omega)$ is define as

$$S(\omega) = \frac{1}{2\pi} \int_{-\infty}^{\infty} R(z) e^{-\omega x} \, dz \tag{6.3}$$

The autocorrelation coefficient is typically characterized by a correlation length, say L_c, which is relate to the distance beyond which the correlation of the material fluctuation diminishes. The correlation length and the form of the autocorrelation function should be determined experimentally either by a direct testing of the material or by an interpretation of the vibration signal. Unfortunately, no such measurement is available to our knowledge [45]. From the material science point of view, L_c should be mainly dependent upon the grain size of the material, hence an estimate can be made.

As a first approximation, a simple but popular model for the autocorrelation coefficient is adopted for the present study [45]:

$$R(z) = e^{\lambda |z|} \tag{6.4}$$

Here, $1/\lambda$ characterizes the correlation length. The power spectral density function corresponding to Equation (6.4) is

$$S(\omega) = \frac{\lambda}{\pi(\lambda^2 + \omega^2)} \tag{6.5}$$

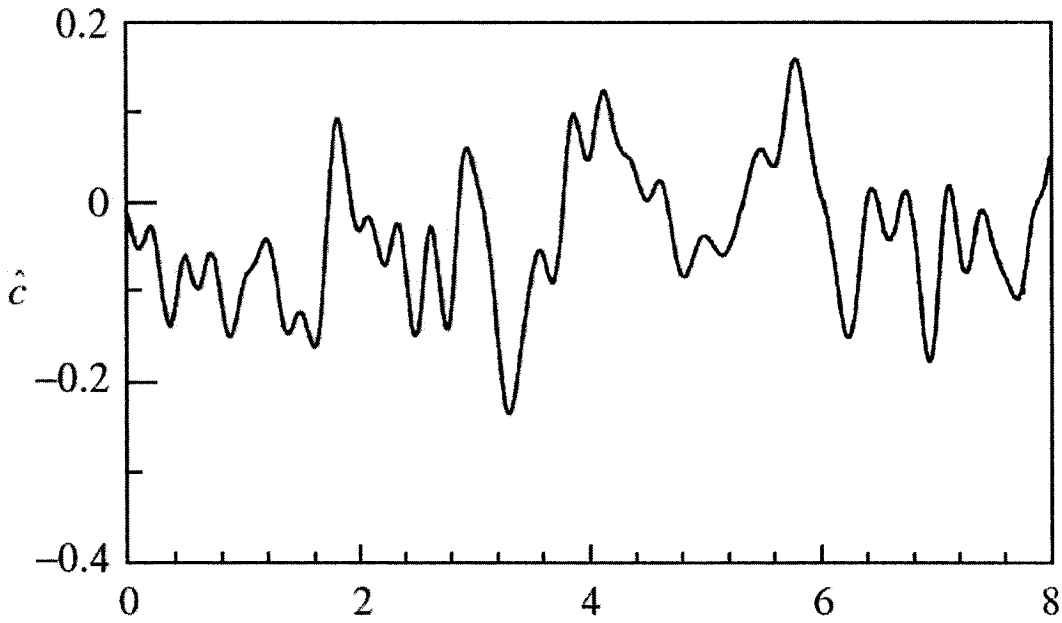

Figure 6.1: A stochastic specific cutting resistance for $\lambda = 5$ [45].

With the above statistical quantities, it is possible to generate artificially a random signal with the same statistics. The technique adopted is the spectral representation method initiated by Rice [33] and refined by Shinozuka et al. [36]. It is modelled by the series

$$\hat{c}(x) = 2\eta \sum_{k=0}^{N-1} \sqrt{S(\omega_k)\Delta\omega cos(\omega_k x + \phi_k)} \tag{6.6}$$

$c(x)$ is shown in Figure 6.1 when $\lambda = 5$, where η is the standard deviation, ϕ_k is a random phase angle uniformly distributed over $[0, 2\pi]$, $\omega_k = k\Delta\omega$, and $\Delta\omega$ is the frequency increment. Assuming the same mathematical model of the MT-CP

system as in the chapter 4 (Equation (4.6) and (4.7)), the cutting forces f_x and f_y depend upon the stochastic properties of the workpiece, which are modelled by the randomness of the specific cutting resistance $c(x)$,

$$f_x(y, x', y') = c(x)q_0h(c_1(abs(v_r) - 1)^2 + 1)H(h), \tag{6.7}$$

$$f_y(y, x', y') = \chi(v_r, v_f, h)f_x(y, x', y'), \tag{6.8}$$

where

$\chi(\cdot) = (c_2(v_f - 1)^2 + 1)(c_3(h - 1)^2 + 1)H(f_x)sgn(v_f)$,

$v_r = v_0 - x'$

$v_f = v_0 - Ry'$,

$h = h_0 - y$,

$R = R_0(c_4(v_r - 1)^2 + 1)$,

$\hat{c}(x) = 2\eta \sum_{k=0}^{N-1} \sqrt{S(\omega_k)\Delta\omega cos(\omega_k x + \phi_k)}$,

$c(x) = \hat{c}(x) + 1$

where h is the depth of cut, v_r is the relative velocity, v_f is friction velocity, $\chi(\cdot)$ is the friction acting on the rake surface. $c_1 - c_4$ and q_0 are cutting parameters. R is shear plastic deformation. m is the vibrating of tool, c_x, c_y are stiffness in x and y direction, k_x, k_y are viscous damping in x and y direction, ω_{0x}, ω_{0y} are natural frequency in x and y direction respectively, α is stiffness ratio, ξ_x, ξ_y are dimensionless coefficient of

viscous damping in x and y direction respectively. $\chi(\cdot)$ is the friction acting on the rake surface. The randomness is introduced by the specific cutting resistance $c(x)$.

6.2 Simulation of the 2D stochastic model

For the stochastic model, $\eta = 0.2$ and $\lambda = 5$ are used. Additional data is $\mu_0 = 0.1$, $c_1 = 0.3$, $c_2 = 0.7$, $c_3 = 1.5$, $c_4 = 1.2$, $R_0 = 2.2$, $\alpha = 4$, $\xi_x = 0.1$, $\xi_y = 0.1$, $h = 0.5$, $q_0 = 1.2$, $v_0 = 0.4$ and $\Delta t = 0.001s$. In the stochastic model the tool undergoes a higher stress, the force can be as much as 300 % to 400 % greater than average value under stead cutting conditions. Figure 6.2 shows the simulation result about cutting forces in x and y directions for the stochastic model. The x component of the cutting force exhibits discontinuities that correspond to the loss of contact between the tool and the workpiece. We observe not only longer transient period, but also much greater impact force than deterministic model. It shows the force can be as much as 300% to 400% greater than average value. The time interval of tool separation is also longer. This theoretical prediction is consistent with the manufacturing reality which the majority of cutting tool breakages occur during the transient period.

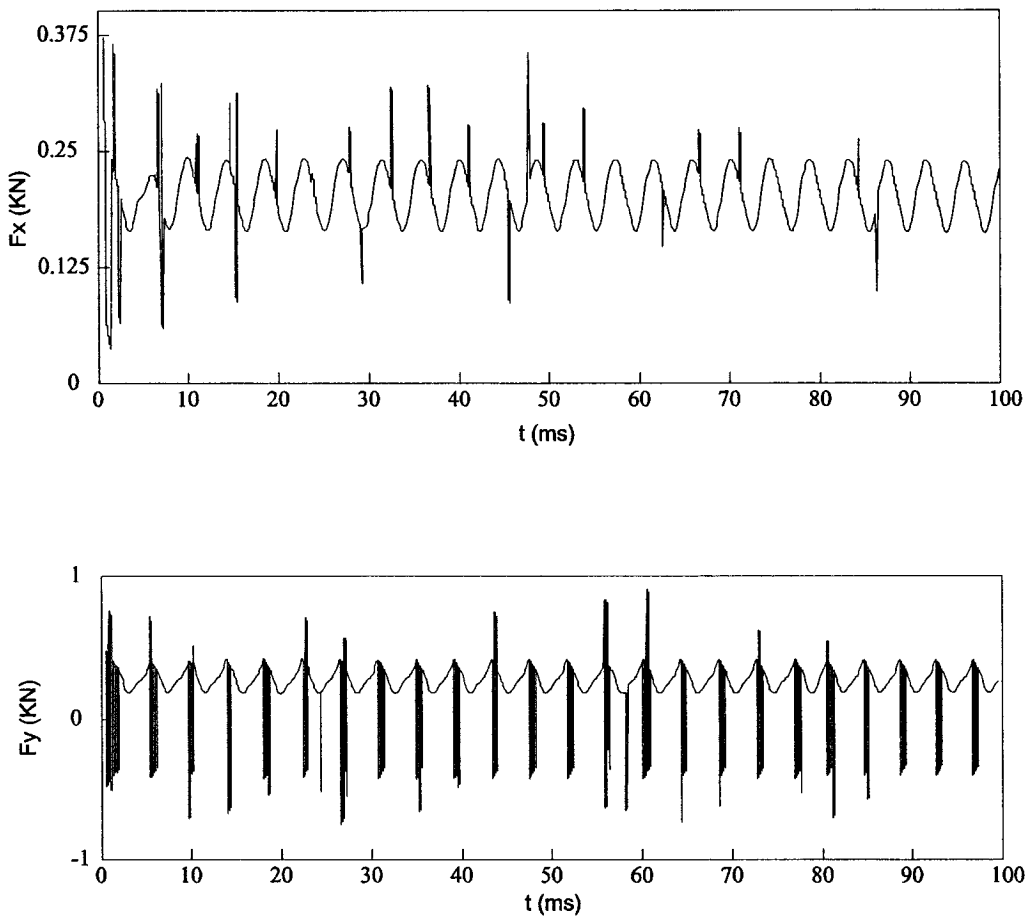

Figure 6.2: f_x and f_y for 2D stochastic model

Chapter 7

Active Control for Chatter with 2-D Stochastic Model and Piezoelectric Actuator

7.1 System Dynamic Model

Form Figure 7.1, the dynamic process of the metal cutting system can be described by a set of two second order differential equations.

$$\begin{bmatrix} 1 & 0 \\ 0 & 1 \end{bmatrix} \begin{bmatrix} x'' \\ y'' \end{bmatrix} + \begin{bmatrix} 2\xi_x & 0 \\ 0 & 2\xi_y\sqrt{\alpha} \end{bmatrix} \begin{bmatrix} x' \\ y' \end{bmatrix} + \begin{bmatrix} 1 & 0 \\ 0 & \alpha \end{bmatrix} \begin{bmatrix} x \\ y \end{bmatrix}$$

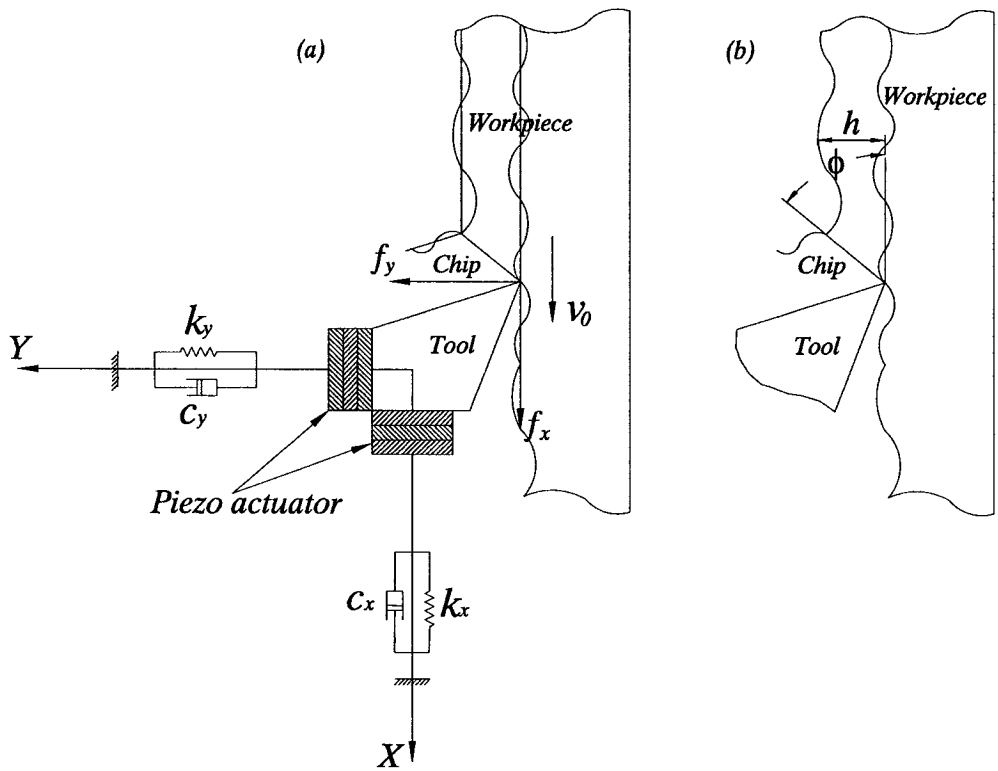

Figure 7.1: Model of cutting system with two piezoelectric actuators

$$= \begin{bmatrix} c(x) \\ \\ \chi(v_r, v_f, h)c(x) \end{bmatrix} f_x(y, x', y') + \begin{bmatrix} 1 & 0 \\ \\ 0 & 1 \end{bmatrix} \begin{bmatrix} f_{px} \\ \\ f_{py} \end{bmatrix} \tag{7.1}$$

$$f_{px} = k_{mpx}[cu_x(t) + d\Big(u_x(t)\Big)] \tag{7.2}$$

$$f_{py} = k_{mpy}[cu_y(t) + d\Big(u_y(t)\Big)] \tag{7.3}$$

$$f_x(y, x', y') = q_0 h(c_1(abs(v_r) - 1)^2 + 1)H(h), \tag{7.4}$$

$$f_y(y, x', y') = \chi(v_r, v_f, h) f_x(y, x', y'), \tag{7.5}$$

where

$\chi() = (c_2(v_f - 1)^2 + 1)(c_3(h - 1)^2 + 1)H(f_x)sgn(v_f)$,

$v_r = v_0 - x'$

$v_f = v_0 - Ry'$,

$h = h_0 - y$,

$R = R_0(c_4(v_r - 1)^2 + 1)$,

$\omega_{0x}^2 = \frac{c_x}{m}$,

$\omega_{0y}^2 = \frac{c_y}{m}$,

$\alpha = \frac{c_y}{c_x}$,

$\xi_x = \frac{k_x}{2m\omega_{0x}}$,

$\xi_y = \frac{k_y}{2m\omega_{0y}}$,

$c(x) = \hat{c}(x) + 1$,

$\hat{c}(x) = 2\eta \sum_{k=0}^{N-1} \sqrt{S(\omega_k)\Delta\omega cos(\omega_k x + \phi_k)}$,

$S(\omega) = \frac{\lambda}{\pi(\lambda^2+\omega^2)}$,

$k_{mpx} = \frac{k_{px}}{m}$,

$k_{mpy} = \frac{k_{py}}{m}$,

where h is the depth of cut, v_r is the relative velocity, v_f is friction velocity, $\chi(\cdot)$ is the friction acting on the rake surface. $c_1 - c_4$ and q_0 are cutting parameters. R is shear plastic deformation. m is the mass of vibrating system, c_x, c_y are stiffness in x and y direction, k_x, k_y are viscous damping in x and y direction, ω_{0x}, ω_{0y} are natural frequency in x and y direction respectively, α is stiffness ratio, ξ_x, ξ_y are dimensionless coefficient of viscous damping in x and y direction respectively. $\chi(\cdot)$ is the friction acting on the rake surface. The randomness is introduced by the specific cutting resistance $c(x)$.

The cutting process starts with an initial depth of cut, h_0, where layers are taken out from the workpiece with the constant velocity, v_0. The rest of the cutting parameters $c_1 - c_4$ and q_0 are constants. η is the standard deviation, ϕ_k is a random phase angle uniformly distributed over $[0, 2\pi]$, $\omega_k = k\Delta\omega$, and $\Delta\omega$ is the frequency increment. For the stochastic model, $\eta = 0.2$ and $\lambda = 5$ are used.

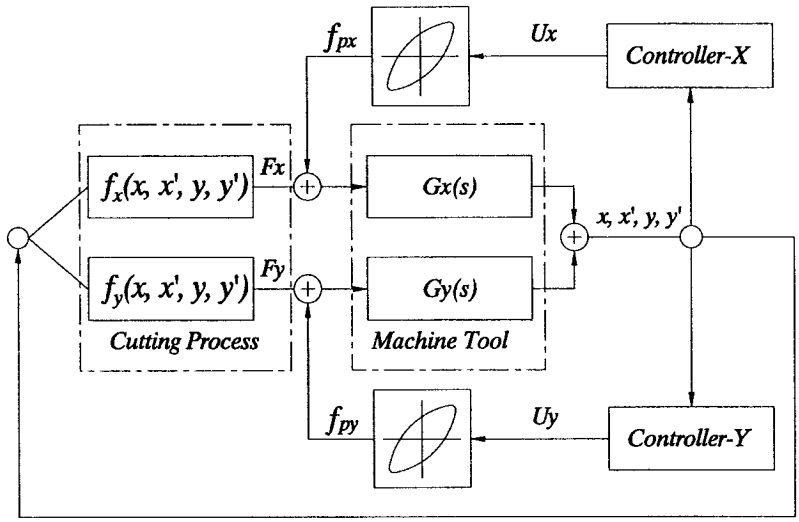

Figure 7.2: Block diagram of turning system with piezoelectric actuators

7.2 Adaptive Controller Design

The closed-loop dynamic system of metal cutting system in turning with piezoelectric actuators and adaptive controllers is illustrated in Figure 7.2.

Equation (7.1) can be transformed as follows:

$$\begin{aligned} x'' + 2\xi_x x' + x &= c(x)q_0(h_0 - y)\left(H(v_0 - x')\frac{1}{1+\mu_0} + sgn(v_0 - x')\frac{\mu_0}{1+\mu_0}\right) \\ &\quad \times\Big(c_1\big(abs(v_0 - x') - 1\big)^2 + 1\Big)H(h_0 - y) + f_{px}, \end{aligned} \tag{7.6}$$

$$y'' + 2\xi_y\sqrt{\alpha}y' + \alpha y = c(x)\Big(c_2(v_0 - Ry' - 1)^2 + 1\Big)\Big(c_3(h_0 - y - 1)^2 + 1\Big)H(f_x)$$

$$\times \left(H(v_0 - x') \frac{1}{1+\mu_0} + sgn(v_0 - x') \frac{\mu_0}{1+\mu_0} \right)$$
$$\times \left(c_1 \Big(abs(v_0 - x') - 1 \Big)^2 + 1 \right) H(h_0 - y)$$
$$\times sgn(v_0 - Ry') q_0(h_0 - y) + f_{py}, \tag{7.7}$$

A filtered tracking error is defined as

$$\delta(t) = \begin{bmatrix} \delta_1(t) \\ \\ \delta_2(t) \end{bmatrix} = \begin{bmatrix} x(t) + \lambda_1 x'(t) \\ \\ y(t) + \lambda_2 y'(t) \end{bmatrix} = 0 \tag{7.8}$$

A turning error δ_ϵ, as follows:

$$\delta_{i\epsilon} = \delta_i - \epsilon \; sat \left(\frac{\delta_i}{\epsilon} \right) \quad i = 1, 2 \tag{7.9}$$

where ϵ is an arbitrary positive constant and $sat(\cdot)$ is the saturation function.

Differentiating $\delta(t)$ with respect to time t as:

So

$$\begin{aligned} \dot{\delta_1}(t) &= (1 - 2\lambda_1 \xi_x) x' - \lambda_1 x + \lambda_1 c(x) q_0(h_0 - y) \\ &\quad \times \left(H(v_0 - x') \frac{1}{1+\mu_0} + sgn(v_0 - x') \frac{\mu_0}{1+\mu_0} \right) \\ &\quad \times \left(c_1 \Big(abs(v_0 - x') - 1 \Big)^2 + 1 \right) H(h_0 - y) \\ &\quad + \lambda_1 k_{mpx} [c u_x(t) + d_x \Big(u_x(t) \Big)], \end{aligned} \tag{7.10}$$

$$\dot{\delta_2}(t) = (1 - 2\lambda_2 \xi_y \sqrt{\alpha}) y' - \lambda_2 \alpha y + \lambda_2 c(x) (c_2 (v_0 - Ry' - 1)^2 + 1)$$

$$\times(c_3(h_0-y-1)^2+1)H(f_x)sgn(v_0-Ry')q_0(h_0-y)$$
$$\times\left(H(v_0-x')\frac{1}{1+\mu_0}+sgn(v_0-x')\frac{\mu_0}{1+\mu_0}\right)$$
$$\times(c_1(abs(v_0-x')-1)^2+1)H(h_0-y)$$
$$+\lambda_2 k_{mpy}[cu_y(t)+d_y\Big(u_y(t)\Big)], \tag{7.11}$$

The above can be simplified:

$$\dot{\delta}_1(t)=\lambda_{x1}x'-\lambda_{x2}x+\eta_x(y)\varsigma_x(x,x')+\lambda_{x3}u_x(t)+\lambda_{x4}d_x\Big(u_x(t)\Big) \tag{7.12}$$

$$\dot{\delta}_2(t)=\lambda_{y1}y'-\lambda_{y2}y+\eta_y(y)\varsigma_y(x,x')+\lambda_{y3}u_y(t)+\lambda_{y4}d_y\Big(u_y(t)\Big), \tag{7.13}$$

where

$$\eta_x(y)=\lambda_1 q_0(h_0-y)H(h_0-y)$$

$$\varsigma_x(x,x')=c(x)\left(H(v_0-x')\frac{1}{1+\mu_0}+sgn(v_0-x')\frac{\mu_0}{1+\mu_0}\right)\left(c_1\Big(abs(v_0-x')-1\Big)^2+1\right)$$

$$\eta_y(y)=\lambda_2(c_2(v_0-Ry'-1)^2+1)(c_3(h_0-y-1)^2+1)sgn(v_0-Ry')q_0(h_0-y)H(h_0-y)$$

$$\varsigma_y(x,x')=c(x)H(f_x)\left(H(v_0-x')\frac{1}{1+\mu_0}+sgn(v_0-x')\frac{\mu_0}{1+\mu_0}\right)(c_1(abs(v_0-x')-1)^2+1)$$

$$\lambda_{x1}=(1-2\lambda_1\xi_x),\ \ \lambda_{x2}=\lambda_1,\ \ \lambda_{x3}=\lambda_1 k_{mpx}c,\ \ \lambda_{x4}=\lambda_1 k_{mpx},$$

$$\lambda_{y1}=1-2\lambda_2\xi_y\sqrt{\alpha},\ \ \lambda_{y2}=\lambda_2\alpha,\ \ \lambda_{y3}=\lambda_2 k_{mpy}c,\ \ \lambda_{y4}=\lambda_2 k_{mpy}$$

Then define

$$\theta_{x1}=\frac{\lambda_{x1}}{\lambda_{x3}},\ \theta_{x2}=\frac{\lambda_{x2}}{\lambda_{x3}},\ \theta_{x3}=\frac{1}{\lambda_{x3}},\ \theta_{x4}=\frac{\lambda_{x4}}{\lambda_{x3}}.$$

$$\theta_{y1} = \frac{\lambda_{y1}}{\lambda_{y3}},\ \theta_{y2} = \frac{\lambda_{y2}}{\lambda_{y3}},\ \theta_{y3} = \frac{1}{\lambda_{y3}},\ \theta_{x4} = \frac{\lambda_{y4}}{\lambda_{y3}}.$$

The following control and adaptation laws are presented:

$$u_x(t) = -\left[k_{x\tau}\delta_1(t) + \hat{\theta}_{x1}x'(t) + \hat{\theta}_{x2}x(t) + \hat{\theta}_{x3}\psi_x(t) + k_x^* sat(\frac{\delta_1(t)}{\epsilon})\right] \tag{7.14}$$

$$u_y(t) = -\left[k_{y\tau}\delta_2(t) + \hat{\theta}_{y1}y'(t) + \hat{\theta}_{y2}y(t) + \hat{\theta}_{y3}\psi_y(t) + k_y^* sat(\frac{\delta_2(t)}{\epsilon})\right] \tag{7.15}$$

$$\psi_x(t) = \eta_x(y)\varsigma_x(x, x') \tag{7.16}$$

$$\psi_y(t) = \eta_y(y)\varsigma_y(x, x') \tag{7.17}$$

$$\dot{\hat{\theta}}_{xi} = proj(\hat{\theta}_{xi},\ -\gamma_{xi}\vartheta_{xi}) \tag{7.18}$$

$$\dot{\hat{\theta}}_{yi} = proj(\hat{\theta}_{yi},\ -\gamma_{yi}\vartheta_{yi}) \tag{7.19}$$

where $k_{x\tau}$ and $k_{y\tau}$ are constant positive gains, and k_x^* and k_y^* are a control gains, satisfying $k_x^* \geq \rho/c_{min}$ and $k_y^* \geq \rho/c_{min}$, whereby, ρ is defined in Equation (2.3). The parameter γ_{xi} and γ_{yi} are positive constants determining the rates of adaptations, the $proj(\cdot,\cdot)$ is a projection operator, which is formulated as follows:

$$proj(\hat{\theta}_{xi},\ -\gamma_{xi}\vartheta_{xi}) = \begin{cases} 0 & : \ if\ \hat{\theta}_{xi} = \theta_{ximax}\ and\ \gamma_{xi}\vartheta_{xi} < 0 \\ -\gamma_{xi}\vartheta_{xi} & : \ if\ [\theta_{ximin} < \hat{\theta}_{xi} < \theta_{ximax}] \\ & : \ or[\hat{\theta}_{xi} = \theta_{ximax}\ and\ \gamma_{xi}\vartheta_{xi} \geq 0] \\ & : \ or\ [\hat{\theta}_{xi} = \theta_{ximin}\ and\ -\gamma_{xi}\vartheta_{xi} \leq 0] \\ 0 & : \ if\ \hat{\theta}_{xi} = \theta_{ximin}\ and\ \gamma_{xi}\vartheta_{xi} > 0 \end{cases} \tag{7.20}$$

where

$\vartheta(t)_{x1} = \delta_{1\epsilon}(t)x'(t),$

$\vartheta(t)_{x2} = \delta_{1\epsilon}(t)x(t),$

$\vartheta(t)_{x3} = \delta_{1\epsilon}(t)\psi_x(t).$

and

$$proj(\hat{\theta}_{yi},\ -\gamma_{yi}\vartheta_{yi}) = \begin{cases} 0 & : \ if\ \hat{\theta}_{yi} = \theta_{yimax}\ and\ \gamma_{yi}\vartheta_{yi} < 0 \\ -\gamma_{yi}\vartheta_{yi} & : \ if\ [\theta_{yimin} < \hat{\theta}_{yi} < \theta_{yimax}] \\ & : \ or[\hat{\theta}_{yi} = \theta_{yimax}\ and\ \gamma_{yi}\vartheta_{yi} \geq 0] \\ & : \ or\ [\hat{\theta}_{yi} = \theta_{yimin}\ and\ -\gamma_{yi}\vartheta_{yi} \leq 0] \\ 0 & : \ if\ \hat{\theta}_{yi} = \theta_{yimin}\ and\ \gamma_{yi}\vartheta_{yi} > 0 \end{cases} \tag{7.21}$$

where

$\vartheta(t)_{y1} = \delta_{2\epsilon}(t)y'(t),$

$\vartheta(t)_{y2} = \delta_{2\epsilon}(t)y(t),$

$\vartheta(t)_{y3} = \delta_{2\epsilon}(t)\psi_y(t).$

7.2.1 Stability Analysis of the System

To establish global boundedness, we define a Lyapunov function candidate :

$$V(t) = \frac{1}{2}\left[\frac{1}{\lambda_{x3}}\delta_{1\epsilon}^2 + \frac{1}{\lambda_{y3}}\delta_{2\epsilon}^2 + \sum_{i=1}^{3}[\frac{1}{\gamma_{xi}}(\hat{\theta}_{xi}(t) - \theta_{xi})^2] + \sum_{i=1}^{3}[\frac{1}{\gamma_{yi}}(\hat{\theta}_{yi}(t) - \theta_{yi})^2]\right] \quad (7.22)$$

i) Since the discontinuity at $|\delta(t)| = \epsilon$ is of the first kind and since $\delta_{i\epsilon}(t) = 0$ when $|\delta(t)| \leq \epsilon$, it follows that the derivative $\dot{V}(t)$ exists for all $\delta(t)$, which is

$$\dot{V}(t) = 0 \quad when\ |\delta(t)| \leq \epsilon. \quad (7.23)$$

ii) When $|\delta(t)| > \epsilon$, using Equation (5.16) and the fact $\delta_{i\epsilon}\dot{\delta}_{i\epsilon} = \delta_{i\epsilon}\dot{\delta}_i$, one has

$$\begin{aligned}
\dot{V}(t) &= \frac{1}{\lambda_{x3}}\delta_{1\epsilon}\dot{\delta}_1 + \sum_{i=1}^{3}[\frac{1}{\gamma_{xi}}(\hat{\theta}_{xi}(t) - \theta_{xi})\dot{\hat{\theta}}_{xi}(t)] \\
&\quad + \frac{1}{\lambda_{y3}}\delta_{2\epsilon}\dot{\delta}_2 + \sum_{i=1}^{3}[\frac{1}{\gamma_{yi}}(\hat{\theta}_{yi}(t) - \theta_{yi})\dot{\hat{\theta}}_{yi}(t)] \\
&= \delta_{1\epsilon}[\theta_{x1}x'(t) + \theta_{x2}x(t) + \theta_{x3}\psi_x(t) + u_x(t) + \theta_{x4}d\big(u_x(t)\big)] \\
&\quad + \sum_{i=1}^{3}[\frac{1}{\gamma_{xi}}(\hat{\theta}_{xi}(t) - \theta_{xi})\dot{\hat{\theta}}_{xi}(t)] \\
&\quad + \delta_{2\epsilon}[\theta_{y1}y'(t) + \theta_{y2}y(t) + \theta_{y3}\psi_y(t) + u_y(t) + \theta_{y4}d\big(u_y(t)\big)] \\
&\quad + \sum_{i=1}^{3}[\frac{1}{\gamma_{yi}}(\hat{\theta}_{yi}(t) - \theta_{yi})\dot{\hat{\theta}}_{yi}(t)] \\
&= \delta_{1\epsilon}[\theta_{x1}x'(t) + \theta_{x2}x(t) + \theta_{x3}\psi_x(t) + \theta_{x4}d\big(u_x(t)\big)] \\
&\quad + \sum_{i=1}^{3}[\frac{1}{\gamma_{xi}}(\hat{\theta}_{xi}(t) - \theta_{xi})\dot{\hat{\theta}}_{xi}(t)] \\
&\quad - \delta_{1\epsilon}\left[k_{x\tau}\delta_1(t) + \hat{\theta}_{x1}x'(t) + \hat{\theta}_{x2}x(t) + \hat{\theta}_{x3}\psi_x(t) + k_x^* sat(\frac{\delta_1(t)}{\epsilon})\right]
\end{aligned}$$

$$
\begin{aligned}
&+\delta_{2\epsilon}[\theta_{y1}y'(t)+\theta_{y2}y(t)+\theta_{y3}\psi_y(t)+\theta_{y4}d\Big(u_y(t)\Big)]\\
&+\sum_{i=1}^{3}[\frac{1}{\gamma_{yi}}(\hat{\theta}_{yi}(t)-\theta_{yi})\dot{\hat{\theta}}_{yi}(t)]\\
&-\delta_{2\epsilon}\left[k_{y\tau}\delta_2(t)+\hat{\theta}_{y1}y'(t)+\hat{\theta}_{y2}y(t)+\hat{\theta}_{y3}\psi_y(t)+k_y^* sat(\frac{\delta_2(t)}{\epsilon})\right] \qquad (7.24)
\end{aligned}
$$

The above equation can be simplified, by the choice of $\delta_{i\epsilon}$, as

$$
\begin{aligned}
\dot{V}(t) \;\leq\; & \delta_{1\epsilon}[\theta_{x1}x'(t)+\theta_{x2}x(t)+\theta_{x3}\psi_x(t)+\theta_{x4}d\Big(u_x(t)\Big)]\\
&+\sum_{i=1}^{3}[\frac{1}{\gamma_{xi}}(\hat{\theta}_{xi}(t)-\theta_{xi})\dot{\hat{\theta}}_{xi}(t)]\\
&-k_{x\tau}\delta_{1\epsilon}^2-\delta_{1\epsilon}\left[\hat{\theta}_{x1}x'(t)+\hat{\theta}_{x2}x(t)+\hat{\theta}_{x3}\psi_x(t)+k_x^* sat(\frac{\delta_1(t)}{\epsilon})\right]\\
&+\delta_{2\epsilon}[\theta_{y1}y'(t)+\theta_{y2}y(t)+\theta_{y3}\psi_y(t)+\theta_{y4}d\Big(u_y(t)\Big)]\\
&+\sum_{i=1}^{3}[\frac{1}{\gamma_{yi}}(\hat{\theta}_{yi}(t)-\theta_{yi})\dot{\hat{\theta}}_{yi}(t)]\\
&-k_{y\tau}\delta_{2\epsilon}^2-\delta_{2\epsilon}\left[\hat{\theta}_{y1}y'(t)+\hat{\theta}_{y2}y(t)+\hat{\theta}_{y3}\psi_y(t)+k_y^* sat(\frac{\delta_2(t)}{\epsilon})\right] \qquad (7.25)
\end{aligned}
$$

By using adaptive laws (5.17), and the properties:

$$
\frac{1}{\gamma_{xi}}(\hat{\theta}_{xi}-\theta_{xi})Proj(\hat{\theta}_{xi},\; -\gamma_{xi}\vartheta_{xi}) \leq (\hat{\theta}_{xi}-\theta_{xi})\vartheta_{xi}
$$

$$
\frac{1}{\gamma_{yi}}(\hat{\theta}_{yi}-\theta_{yi})Proj(\hat{\theta}_{yi},\; -\gamma_{yi}\vartheta_{yi}) \leq (\hat{\theta}_{yi}-\theta_{yi})\vartheta_{yi}
$$

one obtains

$$
\dot{V}(t) \;\leq\; \delta_{1\epsilon}\left[\theta_{x1}x'(t)+\theta_{x2}x(t)+\theta_{x3}\psi_x(t)+\theta_{x4}d\Big(u_x(t)\Big)\right]
$$

$$
\begin{aligned}
&+(\hat{\theta}_{x1}-\theta_{x1})\delta_{1\epsilon}x'(t)+(\hat{\theta}_{x2}-\theta_{x2})\delta_{1\epsilon}x(t)+(\hat{\theta}_{x3}-\theta_{x3})\delta_{1\epsilon}\psi_x(t)\\
&-k_{x\tau}\delta_{1\epsilon}^2-\delta_{1\epsilon}\left[\hat{\theta}_{x1}x'(t)+\hat{\theta}_{x2}x(t)+\hat{\theta}_{x3}\psi_x(t)+k_x^* sat(\frac{\delta_1(t)}{\epsilon})\right]\\
&+\delta_{2\epsilon}\left[\theta_{y1}y'(t)+\theta_{y2}y(t)+\theta_{y3}\psi_y(t)+\theta_{y4}d\Big(u_y(t)\Big)\right]\\
&+(\hat{\theta}_{y1}-\theta_{y1})\delta_{2\epsilon}y'(t)+(\hat{\theta}_{y2}-\theta_{y2})\delta_{2\epsilon}y(t)+(\hat{\theta}_{y3}-\theta_{y3})\delta_{2\epsilon}\psi_y(t)\\
&-k_{y\tau}\delta_{2\epsilon}^2-\delta_{2\epsilon}\left[\hat{\theta}_{y1}y'(t)+\hat{\theta}_{y2}y(t)+\hat{\theta}_{y3}\psi_y(t)+k_y^* sat(\frac{\delta_2(t)}{\epsilon})\right]\\
=\;&-k_{x\tau}\delta_{1\epsilon}^2-k_x^*\delta_{1\epsilon}sat(\frac{\delta_1(t)}{\epsilon})+\theta_{x4}\delta_{1\epsilon}d\Big(u_x(t)\Big)\\
&-k_{y\tau}\delta_{2\epsilon}^2-k_y^*\delta_{2\epsilon}sat(\frac{\delta_2(t)}{\epsilon})+\theta_{y4}\delta_{2\epsilon}d\Big(u_y(t)\Big) \qquad (7.26)
\end{aligned}
$$

Since $|\delta_{i\epsilon}| = \delta_{i\epsilon}sat(\frac{\delta_i}{\epsilon})$ for $|\delta_i| > \epsilon$, $||d(u_x(t))|| \leq \rho$ and $||d(u_y(t))|| \leq \rho$ the above becomes

$$
\begin{aligned}
\dot{V}(t) \;\leq\;& -k_{x\tau}\delta_{1\epsilon}^2-k_x^*|\delta_{1\epsilon}|+\theta_{x4}d\Big(u_x(t)\Big)|\delta_{1\epsilon}|\\
&-k_{x\tau}\delta_{1\epsilon}^2-k_x^*|\delta_{1\epsilon}|+\theta_{x4}d\Big(u_x(t)\Big)|\delta_{1\epsilon}| \qquad (7.27)
\end{aligned}
$$

Then we define $k_x^* = k_{xmax}^* \geq \rho\theta_{xmax}$ and $k_y^* = k_{ymax}^* \geq \rho\theta_{ymax}$ we will get

$$
\begin{aligned}
\dot{V}(t) \;\leq\;& -k_{x\tau}\delta_{1\epsilon}^2-k_x^*|\delta_{1\epsilon}|+\theta_{x4}d\Big(u_x(t)\Big)|\delta_{1\epsilon}|\\
&-k_{x\tau}\delta_{1\epsilon}^2-k_x^*|\delta_{1\epsilon}|+\theta_{x4}d\Big(u_x(t)\Big)|\delta_{1\epsilon}|\\
\leq\;& -k_{x\tau}\delta_{1\epsilon}^2-k_{y\tau}\delta_{2\epsilon}^2 \qquad (7.28)
\end{aligned}
$$

7.2.2 Simulation of the Dynamic System

To suppress the chatter the adaptive control law (Equation (7.21)) are introduced into the system (Equation (7.1)). The parameters limits are $\theta_{x1} \in [-4.5e(-4), -2.5e(-4)]$, $\theta_{x2} \in [3.5e(-4), 2.0e(-4)]$, $\theta_{x3} \in [-4.2e(-4), -2.2e(-4)]$, $\theta_{x4} \in [5.0e(-4), 1.5e(-3)]$, $\theta_{y1} \in [-5.5e(-4), -3.5e(-4)]$, $\theta_{y2} \in [4.0e(-4), 6.5e(-4)]$, $\theta_{y3} \in [-5.5e(-4), -2.5e(-4)]$, $\theta_{y4} \in [5.0e(-4), 1.5e(-3)]$. Then we are taking initial data as $\theta_{x1} = -3.85e(-4)$, $\theta_{x2} = 1.4e(-4)$, $\theta_{x3} = -3.57e(-4)$, $\theta_{x4} = 1.0e(-3)$, $\theta_{y1} = -4.9e(-4)$, $\theta_{y2} = 5.7e(-4)$, $\theta_{y3} = -4.3e(-4)$, $\theta_{y4} = 1.0e(-3)$, $\gamma_{xi} = 1$ $(i = 1, 2, 3)$, $\gamma_{yi} = 1$ $(i = 1, 2, 3)$, $\epsilon = 1.0e(-4)$ and $K_\tau = 2.0e(-4)$. For the stochastic model, $\eta = 0.2$ and $\lambda = 5$ are used. For a given set of parameters and initial condition, the numerical integration is carried out using the fourth-order Runge-Kutta procedure with a fixed time-step, $\Delta t = 0.001s$. Because when the discontinuity occurs, Additional data is $\mu_0 = 0.1$, $c_1 = 0.3$, $c_2 = 0.7$, $c_3 = 1.5$, $c_4 = 1.2$, $R_0 = 2.2$, $\alpha = 4$, $\xi_x = 0.1$, $\xi_y = 0.1$, $h = 0.5$, $q_0 = 1.2$, $v_0 = 0.4$ and $\Delta\tau = 0.001s$. Figure 7.2 and Figure 7.3 show the simulation results for the chatter suppression in 2D Stochastic model. In Figure 7.2 the F_x and F_y will be stable due to the adjustment by piezoelectric actuator. Finally the U_x and U_y were shown in Figure 7.3.

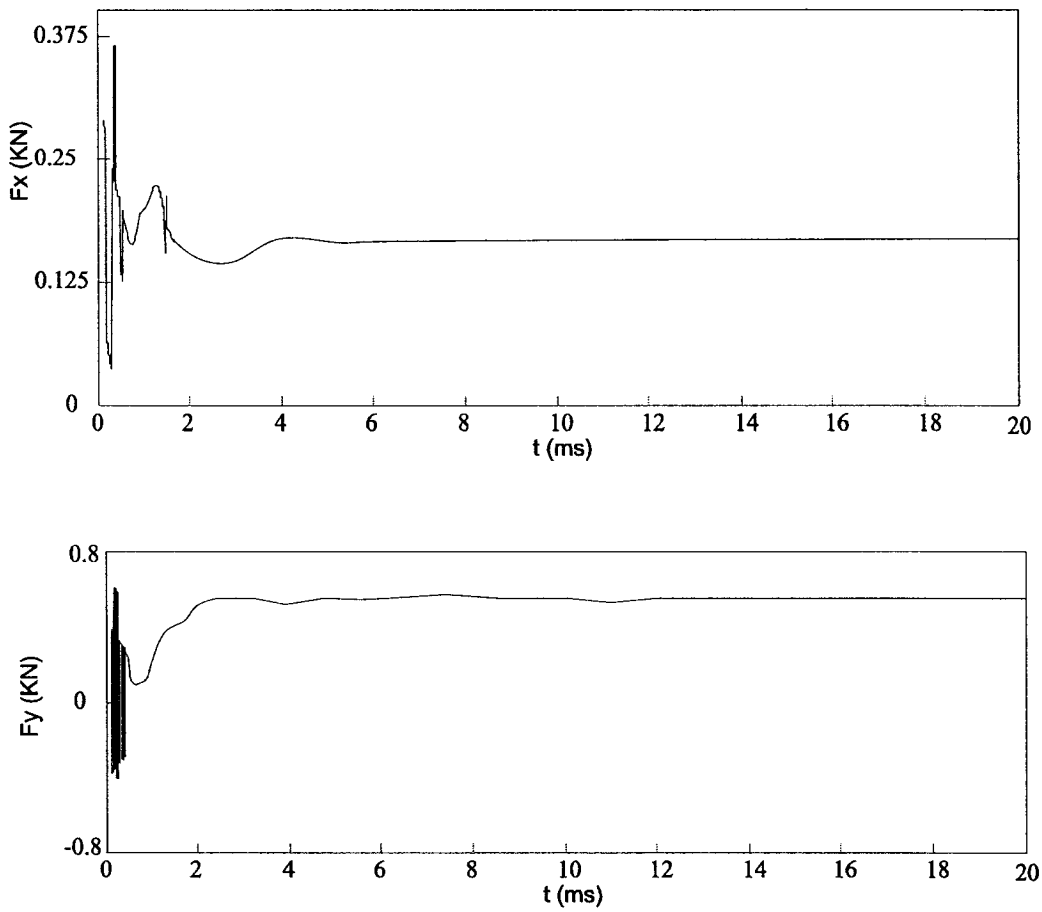

Figure 7.3: F_x and F_y of the adaptive control system

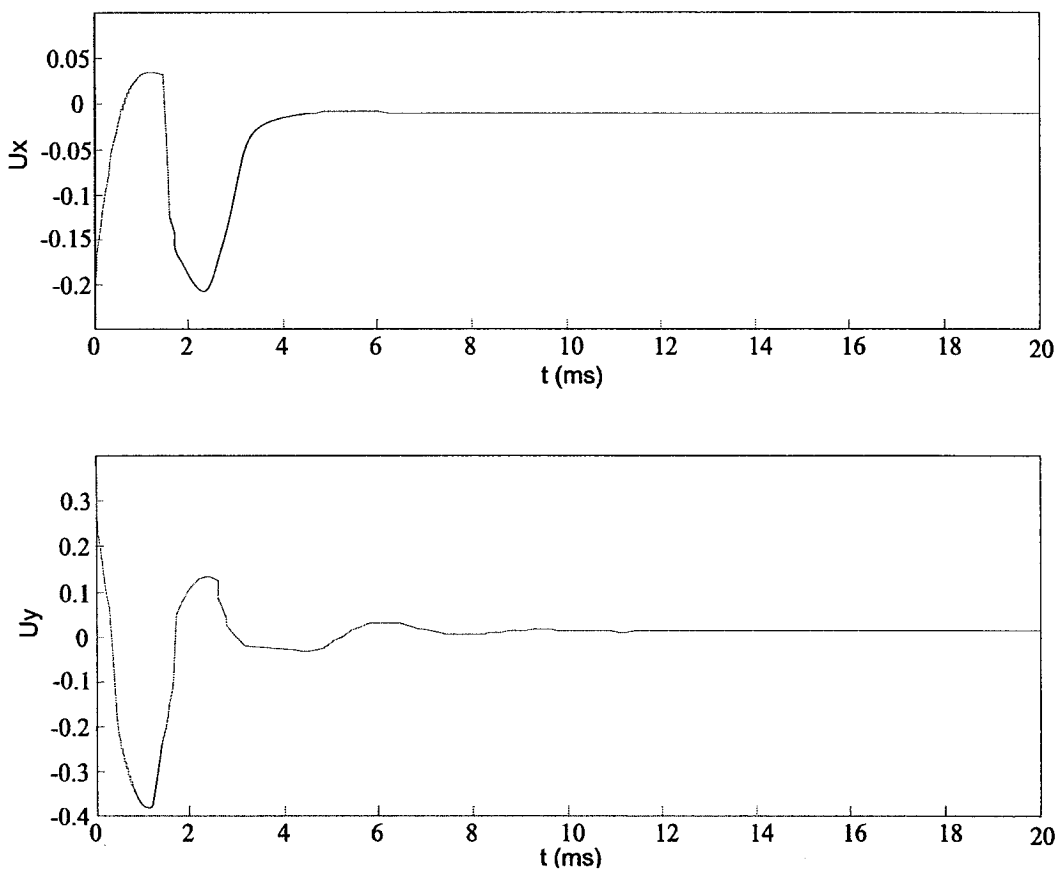

Figure 7.4: U_x and U_y of the adaptive control system

Chapter 8

Conclusion and Future Works

8.1 Conclusion

In this thesis, frictional and impact dynamic models of the orthogonal metal cutting generating chatter were examined. And the piezoelectric actuators are introduced to suppress the chatter because of the advantages of piezoelectric actuator.

The system demonstrates a complex dynamic behavior, which is manifested by the existence of periodic, quasi-periodic, subharmonic and chaotic motion. And the introduction of stochastic model can show there is an immense increase in the cutting forces (up to 300%) during the initial period of cutting. This could explain the in-

dustrial reality, where the majority of the catastrophic tool breakage occurs during this initial stage. That feature is not present in the deterministic model.

In general, it may be concludes that the nonlinear dynamic responses of the system can be controlled most effectively by piezoelectric actuator. Unlike traditionally discontinuous model for backlash hysteresis, a continuous-time model for backlash hysteresis model by Su *et. al.*[38] is used to explain the nonlinear MT-CP system. In this thesis, with the application of piezoelectric actuators in two directions x and y, we develop a adaptive controller to deal with unknown hysteresis. According to my knowledge there is no discussion in the literature about frictional and impact chatter suppression by piezoelectric actuator. It is the first time that the frictional and impact chatter was combined with an adaptive control system of nonlinear system with unknown hysteresis by using a piezoelectric actuator. And the results of simulating for adaptive control laws show that it is effective to suppress the chatter by the piezoelectric actuators.

8.2 Future Works

In this study the adaptive control methods are investigated for the frictional and impact chatter in orthogonal cutting with two-degree-of-freedom deterministic and stochastic models. In the future works three-degree-of-freedom models in 3D metal cutting are recommended.

In the present investigation for the two-degree-of-freedom stochastic system we only consider the cutting resistance as a one-dimensional process, $c(x)$, because it is a reasonable approximation for orthogonal cutting. But for 3D metal cutting the cutting resistance should be considered as a three-dimensional process $c(r)$, where $r(t) = (x(t), y(t), z(t)$ is a parametric function of time.

The future works should pay more attention to the thermomechanical chatter. Not only all kinds of cutting forces and frictions can cause chatter, but also the thermodynamics of chip formation. In reality there are functional interrelationships between the two systems, mechanics and thermodynamics of chip formation [47]. In the future works the complex models including mechanics and thermodynamics of chip formation are recommended.

Finally, once the controller are presented through analytical investigation, a prototype may be tested in the laboratory and in the field to confirm the analysis.

Bibliography

[1] Arnold, R. N., Mechanism of Tool Vibration in Cutting Steel. Proc. Inst. Mech. Engrs. 154, 261-276,1946.

[2] Boothroya, G., Fundamentals of Metal Machining and Machine Tools. McGraw-Hill, 1975.

[3] Chen, B. S. and Chang, Y. F. Robust PI Control Design for a Constant Turing Force System. Int. J. Machine Tools Manfuacture, Vol. 31, 257-272, 1991.

[4] Cook, N. H., Self-excited Vibrations in Metal Cutting. Trans. ASME J.Engng industry 81, 183-186, 1959.

[5] Cuttino, J.F., Miller, A. C. Schinstock, D. E., Performance Optimization of a Fast Tool Servo for Single-Point Diamand Turning Machines, IEEE/ASME Trans Mechatronics, Vol. 4, 169-178, 1999

[6] Davies, M. A., Burns, T. J. and Evans, C. J., On the Dynamics of Chip Formation in Machining Hard Materials. Ann. CIRP 46, 25-30, 1997.

[7] Doi, S. & Kato, S., Chatter Vibration of Lathe Tools. Trans. ASME 78, 1127-1134, 1956.

[8] Fawcett, S. C., Small Amplitude Vibration Compensation for Precision Diamand Turning, Precision Eng., Vol. 12, No.2, 1990.

[9] Ge, P., Morris, K. A., Wang, D. W. L., Passivity-Based Stability and Control of Hysteresis in Smart Actuators. IEEE Trans. Control System Technology, Vol. 9, No.1, 5-16, 2001.

[10] Grabec, I., Chaotic Dynamics of the Cutting Process. Int. J. Mech. Tools manufact. 28, 19-32, 1988.

[11] Hahn, R. S., Metal-cutting Chatter and Its Elimination. Trans. ASME 75, 1073-1080, 1953.

[12] Hamdan, M. N., & Bayoumi, A. E., An Approch to Study the Effects of Tool gemetry on the Primary Chatter Vibration in Orthogonal Cutting. J. Sound Vib 128, 452-469, 1989.

[13] Hastings, W.F., Mathew, P. & Oxley, P.L.B., A Machining Theory for Predicting Chip Geometry, Cutting Forces, etc., From Material Properties and Cuting Conditions. Proc. R. Soc. Lond. A 371, 569-587, 1980.

[14] Hwang, H. Y., Oh, J. H., Kim, K. J., Modeling and Adaotive Pole Assignment Control in Turning. Int. J. Machine Tools Manufacture, Vol.29, 275-285, 1989.

[15] Jang, J. L., Tarng, Y. S. A Study of the Active Vibration Control of a Cutting Tool. Journal of Materials Processing Technology. 95 pp. 78-82, 1999.

[16] Jemielniak, K. &widota, A., Numerical Simulation on Non-linear Chatter Vibration in Truning. Int. J. Mach. Tools Manufact. 29, 239-247, 1988.

[17] Kaneko, T., Sato, H., Tani, Y. & O-hori, M., Self-excited Chatter and Its Marks in Turning. Trans. ASME J. Engng Industry 106, 222-228, 1984

[18] Kegg, R. L., Cutting Dynamics in Machine Tool Chatter. Trans. ASME J. Engng Industry 87, 464-470, 1965.

[19] Kudinov, V.A., Dynamic Characteristics of the Metal Cutting Process. Stanki i Instrument 10, 1-7, 1963.

[20] Lin, J. S., Wneg, C. I. A Nonlinear Dynamic Model of Cutting. International Journal of Machine Tools Manufacture, Vol.30, 53-64, 1990.

[21] Liu, D., Sutherland, J. W., Moon, K. S., Sturos, T. J., Kashani, A. R. Surface Texture Improvement in the Turning Process Via Application of a Magnetostrictively Actuated Tool Holder. J. of Dynamic Systems, Measurement, and Control, Vol. 120, 193-199, 1998.

[22] Lee, B. Y., Tarng, Y. S., Ma, S. C., Modelling of the Process Damping Force in Chatter Vibration. Int. J. Mach. Tools Manufact. 35(7) pp. 951-962, 1995.

[23] Lin, J. S. & Weng, C. I., Nonlinear Dynamics of the Cutting Process. Int. J. Mech. Sci. 33, 645-657, 1991.

[24] Marui, E., Kato, S., Hashimoto, M. & Yamada, T., The Mechanicsm of Chatter in a Spondle Workpiece System. Part 1. Properties of Self-excited Vibration in Spindle Workpiece System. Trans. ASME J.Engng Industry 110, 236-241, 1988.

[25] Merchant, M.E., Basic Mechanics in the Metal Cutting Process. Trans. ASME J.Appl. Mech. 168, 168-175, 1944.

[26] Merritt, H.E., Theory of Self-excited Machine-tool Chatter. Trans. ASME J.Engng Industry 87, 447-454, 1965.

[27] Nelison, R. D., and Gonzalves, D. H., Chaotic Motion of a Rotor System with a Bearing Clearance. Application Fractals and Chaos., pp 285-303, 1993.

[28] Nordkmark, A. B., Non-Periodic Motion Caused by Grazing Incidence in a Impact Oscillator. J. Sound and Vibration, Vol145, No. 2, pp, 279-297, 1991.

[29] Opitz, H. & Bernardi, F., Investigation and Calculation of the Chatter Behavior Lathes and Milling Machines. CIRP 18, 335-343, 1970.

[30] Oxley, P.L.B., Shear Angle Solution Based on Experimental Shear Zone and Tool-Chip Interface Stress Distribution. Int. J.mech. Sci.5, 41-47, 1963.

[31] Rasmussen, J. D., Tsao, T. C. Hanson, R. D., Kapoor, S. G., Dynamic Variable Depth of Cut Machining Using Piezoelectric Actuators. Int. J. Machine Tools Manufacture, Vol. 34, 379-392, 1994.

[32] Recht, R.F., A Dynamic Analysis of High-speed Machining. Trans. ASME J. Engng Industry 107, 309-315, 1985.

[33] Rice, S. O., Mathematical Analysis and Random Noise. In Select Papers on Noise and Stochastic Processes. ed. N. Wax. Dover, New York, pp. 133-294, 1954.

[34] Richter, H., Misawa, E. A., Lucca, D.A., Lu, H., Modeling Nonlinear Behavior in a Piezoelectric Actuator. Precision Engineering. 25. 128-137, 2001.

[35] Shaw, S. W. and Holmes, P. J., A Periodically Forced Piecewise Linear Oscillator, J. Sound and Vibration, Vol 90, No. 1, pp. 129-155, 1983.

[36] Shinozuka, M. and Jan, C. M., Digital Simulation of Random Processes and its Applications. J. Sound Vibration. 251, 111-128, 1973.

[37] Shiraishi, M., Yamanaka, K., and Fujita, H., Optimal Control of Chatter in Turning. Int. J. Mach. Tools Manufact. Vol. 31. pp. 31-43, 1991.

[38] Su, C. Y., Stepanenko, Y., Jaroslav, S., Leung, T. P., Robust Adaptive Control of A Class of Nonlinear Systems with Unknown Backlash-like Hysteresis. IEEE Transactions on Automatic Control, Vol 45, No.12, 2427-2432, 2000.

[39] Tarng, Y. S., Wang. Y. S., An Adaptive Fuzzy Control System for Turning Operations, Int. J. Machine Tools Manufacture, Vol.33, 761-771, 1993.

[40] Tlusty, J. & polacek, M., The Stability of Machine Tools Against Self Excited Vibrations in Machining. In International Research in Production Engineering, pp. 465-474. ASME, 1963.

[41] Tobias, S. A. & Fishwick, W., The Chatter of Lathe Tools Under Orthogonal Cutting Conditions Trans. ASME 80, 1079-1088, 1958.

[42] Warminski, J. and litak, G., Approximate Analytical Solutions for Primary Chatter in the Non-linear Metal Cutting Model. Journal of Sound and Vibration 259, 917-933, 2003.

[43] Wu, D. W., Comprehensive Dynamic Cutting Force Model and its Application to Wave-removing Process. Trans. AMSE J. Engng Industry 108, 281-287, 1988.

[44] Wu, D. W., Liu, C. R., An Analytical Model of Cutting Dynamics. Part 2. Verification. trans. ASME J. Engng Industry 107, 107-111, 1985.

[45] Wiercigroch, M., Cheng, A. D. H., Chaotic and Stochastic Dynamics of Othogonal Metal Cutting. Chaos Solitons Fractals 8, 715-726, 1997.

[46] Wiercigroch, M., Chaotic Vibrations of a Simply Model of the Machine Tool-cutting Process System. Archive Mech. Engng 42, 151-165, 1997.

[47] Wiercigroch, M., Budak, E., Sources of Nonlinearities, Chatter Generation and Suppression in Metal Cutting. Phil. Trans. R. Soc. Lond. A 359, 663-693, 2001.

[48] Yang, X. G., Eman, K. F., Wu, S. M., Analysis of Three-Dimensional Cutting Process Dynamics. Transactions of the ASME. Vol. 107 pp 336-341, 1985.

[49] Piezoelectric and Electrostrictive Ceramics, Http://www.piezomechanik.com.

Appendix A

Merchant's Model

In the pioneering work of Merchant [25], a model of the cutting process was used in which the shear in chip formation was confined to the shear plane, and movement of the chip over the tool occurred by classic sliding friction, defined by an average friction angle β. Merchant's force circle were restricted to a model of orthogonal or two-dimensional metal cutting shown in Figure 1 [25].

The forces can be found from Figure 1 as the two equations below:

$$F_c = \frac{h_0\, w\, k\, cos(\beta - \alpha)}{sin\phi\, cos(\phi + \beta - \alpha)} \tag{1}$$

$$F_t = \frac{h_0\, w\, k\, sin(\beta - \alpha)}{sin\phi\, cos(\phi + \beta - \alpha)} \tag{2}$$

where h_0 is the initial depth of cut and β is an average friction angle.

Differentiating the first equation with respect to the shear plane angle gives:

$$\frac{dF_c}{d\phi} = \frac{h_0\, w\, k\, cos(\beta - \alpha)\, cos(2\phi + \beta - \alpha)}{sin^2\phi\, cos^2(\phi + \beta - \alpha)} \tag{3}$$

and the Merchant equation as

$$\phi = \frac{\pi}{4} - \frac{1}{2}\beta + \frac{1}{2}\alpha \tag{4}$$

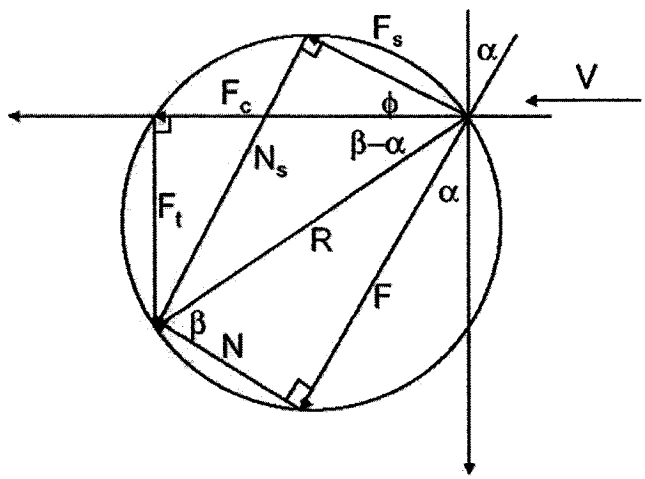

Figure 1: Merchant's force diagram [25]

For the main cutting force F_c acting in the tool work direction:

$$F_c = \frac{h_0\, w\, k\, cos(\beta - \alpha)}{sin\left[\frac{\pi}{4} - \frac{1}{2}(\beta - \alpha)\right]\, cos\left(\frac{\pi}{4} + \frac{1}{2}\beta + \frac{3}{2}\alpha\right)} \tag{5}$$

From trigonometry the main cutting force can be written as:

$$F_c = 2\, w\, h_0\, k\, cot\phi \tag{6}$$

The feed force acting normal to the main cutting force is:

$$F_t = \frac{h_0\, w\, k\, sin(\beta - \alpha)}{sin\left(\frac{\pi}{4} - \frac{1}{2}(\beta - \alpha)\right)\, cos\left(\frac{\pi}{4} + \frac{1}{2}\beta + \frac{3}{2}\alpha\right)} \tag{7}$$

And from the force diagram the forces on the shear plane are given by

$$F_s = F_c\, cos\phi - F_t\, sin\phi \tag{8}$$

$$F_N = F_c \, sin\phi + F_t \, cos\phi \tag{9}$$

The shear stress and normal stress are given by

$$K_s = \frac{F_s}{A_s} = \frac{[F_c \, cos\phi - F_t \, sin\phi] \, sin\phi}{w \, h_0} \tag{10}$$

$$\sigma = \frac{F_N}{A_s} = \frac{[F_c \, sin\phi + F_t \, cos\phi] \, sin\phi}{w \, h_0} \tag{11}$$

where F_s is shear force, f_N is normal force, K_s is shear stress, σ is normal stress, A_s is the shear-plane area $wh_0/sin\phi$.

The coefficient of friction is defined as the ratio of the force in the direction of sliding to the force normal to the sliding interface. From Figure 1 the coefficient of friction was shown as

$$\mu = \frac{F}{N} = \frac{F_c \, sin\phi + F_t \, cos\phi}{F_c \, cos\phi - F_t \, sin\phi} = \frac{F_c + F_t tan\alpha}{F_c - F_t tan\alpha} = tan\beta \tag{12}$$

where μ is coefficient of friction, F is the friction force on the rake face shown in the Figure 1, N is the normal force on the rake face, and β is the friction angle.

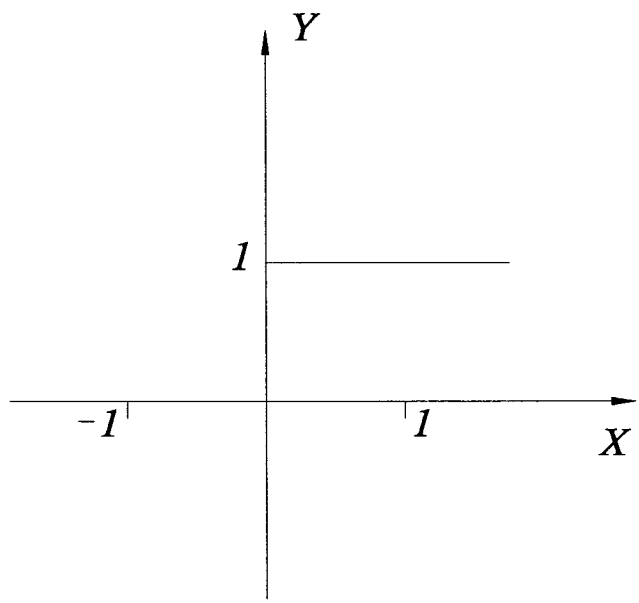

Figure 2: The Heaviside function

Appendix B

Heaviside Function

Shown in Figure 2, the (unit) Heaviside function $H(x)$ can be defined by either of:

$$H(x) = \begin{cases} 1 & x > 0 \\ 0 & x < 0 \end{cases} \tag{13}$$

or

$$\int_{-\infty}^{\infty} H(x)\phi(x)dx = \int_{0}^{\infty} \phi(x)dx \tag{14}$$

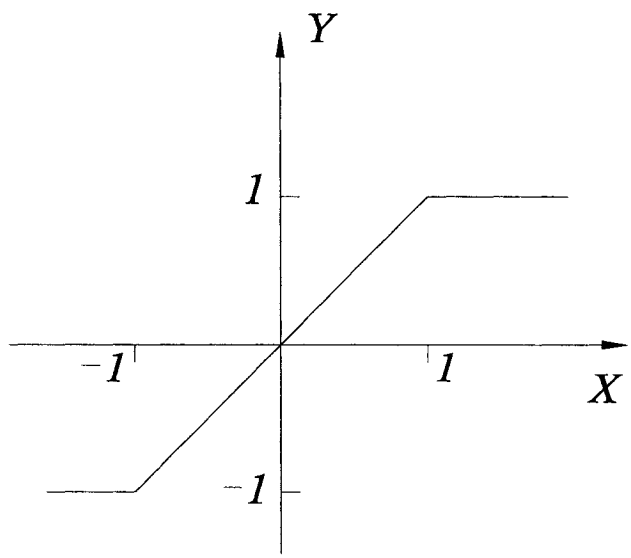

Figure 3: The Saturation function

Appendix C

Saturation Function

Shown in Figure 3, the Saturation function $sat(x)$ can be defined by

$$sat(x) = \begin{cases} x & |x| < 1 \\ 1 & x \geq 1 \\ -1 & x \leq -1 \end{cases} \tag{15}$$